SLAC-PUB-2607
September 1980
(T/E)

QUARKS AND GLUONS IN LOW-p_T PHYSICS*

J. F. Gunion
Stanford Linear Accelerator Center
Stanford University, Stanford, California 94305
and
University of California at Davis
Physics Department, Davis, California 95616

Abstract

We review and comment on some of the existing approaches to low-p_T particle production based on ideas of quantum chromodynamics. We focus on the relationships between the various theories and, in particular, note the points of overlap between them. Constraints upon the models coming from deep inelastic and e^+e^- annihilation data are discussed.

In the last eight years high energy physics has focused upon successfully understanding short distance physics using the theory of quantum chromodynamics (QCD). The use of QCD to understand low-p_T hadronic physics is, in contrast, plagued with many uncertainties. Nonetheless developments over the last few years suggest that many of the regularities of hadronic low-p_T reactions can be related to the underlying presence of quarks and gluon induced reactions between them. It is the purpose of this talk to review some of the models proposed in the literature, to discuss the constraints imposed upon them by data from the short-distance, deep-inelastic and e^+e^- annihilation realm, and to comment upon their internal self-consistency as well as the relationship between various models. In particular considerable effort is devoted to pedagogical explanations of essential features and ingredients.

The outline of the talk is as follows:

---

* Work supported in part by the Department of Energy, contract DE-AC03-76SF00515 and in part by the Alfred P. Sloan Foundation.

(Presented at the XI International Symposium on Multi-Particle Dynamics, Bruges, Belgium, June 22-27, 1980.)

I. Interactions Between Hadrons

A) Elementary QCD Exchange Possibilities

Before one can discuss the structure of the final state in a hadron-hadron collision it is, of course, necessary to have a relatively precise picture of the interaction mechanism

responsible for causing a collision at low-p_T. Various pictures have been proposed over the years. The two most elementary QCD mechanisms which yield an approximately constant total cross section are: 1) gluon exchange[1] and 2) slow or "wee" quark exchange.[2] These are pictured in Fig. 1(a) and (b). Both have many of the same features as the dual model cylinder diagram

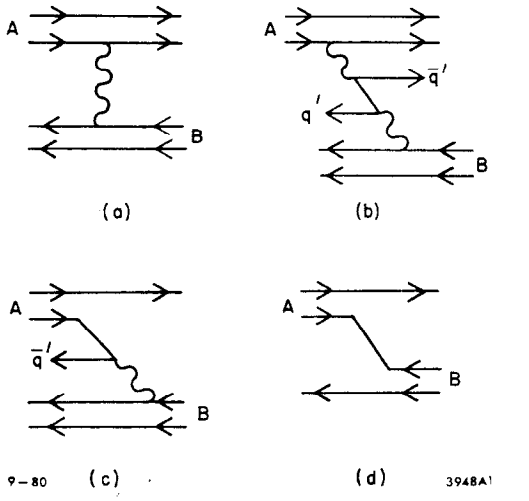

Fig. 1. The interaction between two meson states due to: a) gluon exchange; b) slow "sea" quark exchange; c) slow B-quark absorption of a valence quark in A — the reverse diagram also occurs; d) valence quark exchange.

picture of the Pomeranchuk-Regge trajectory, which underlies many of the low-p_T particle production theories.[3,4,5] In both cases the gluon(s) guarantee zero flavor quantum number exchange and, because of their vector nature, a constant or logarithmically rising total cross section. Note that in Fig. 1(b) based on "sea" quark exchange we have a slow "sea" quark in A interacting with a slow "sea" antiquark in B. A constant cross section is also obtained from Fig. 1(c) in which a "sea" quark in B interacts with a valence quark in A. This diagram is not symmetric between its forward and backward fragmentation which is probably ruled out experimentally.[1,6] More discussion will be given later in Sec. III. A valence-on-valence interaction as in Fig. 1(d) cannot yield a constant cross section, and will be henceforth eliminated from discussion. It may play a subassymptotic role in πp and $\bar{p}p$ reactions. Of course more complicated versions of (a)-(c) are possible employing higher Fock states of the incoming hadrons A and B. Examples are given in Fig. 2(a)-(c).

Fig. 2. Examples of a) gluon exchange; b) "sea" quark exchange; and c) slow quark absorption of a valence quark, employing higher Fock states for A and/or B.

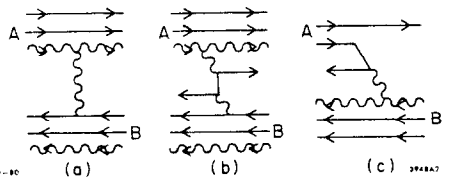

In general there are clearly many such diagrams to consider. All contributions of type (a) and (b), however, yield two important general features.[8]

1) Given a Fock state of A(B) with $n_q^A(n_q^B)$ quarks (plus antiquarks) and $n_g^A(n_g^B)$ gluons, we find that

$$\sigma_T = \sum_{\substack{\text{Fock} \\ \text{states}}} \left(n_q^A + \frac{9}{4} n_g^A\right)\left(n_q^B + \frac{9}{4} n_g^B\right) c_{AB} \qquad (1.1)$$

This is a generalization of quark counting. (The 9/4 represents the larger effective color "charge" squared of a constituent gluon, compared to a quark, as seen by the exchanged or bremstrahlunged gluon in mechanism (a) or (b), respectively.) It assumes a similar relative transverse momentum, k_t, distribution for all quarks and gluons in a given Fock state; the constant, c_{AB}, is determined by a convolution of k_t^A and k_t^B distributions. In addition, gluon bremstrahlung models suggest that

$$\langle n_q^A \rangle = n_{\text{valence}}^A (1 + 2c) \ , \qquad \langle n_g^A \rangle = n_{\text{valence}}^A \ c' \ ; \qquad (1.2)$$

that is the number of sea $q\bar{q}$ pairs and the number of gluons in the Fock states are proportional to the original valence quark number. If this is true and if c_{AB} is not rapidly varying between Fock states then one obtains

$$\sigma_T \propto n_{\text{valence}}^A \ n_{\text{valence}}^B \qquad (1.3)$$

as found to be approximately true experimentally. Quark counting also clearly holds for mechanism (c) in the same approximation; however it does not generally hold for mechanism (d) due to the absence of antiquarks in the proton valence state. It is also true that the calculated size of c_{AB} and hence σ_T is reasonable for the expected forms of the k_t^A and k_t^B distributions and a moderate value of α_s ($\alpha_s \gtrsim .5$) at low momentum transfer.

2) Mechanisms (a) and (b) are sensitive to the size of the colliding bound states. Given a fixed target, B, the smaller the bounds state size of A, $\langle r_A^2 \rangle$, the smaller the constant c_{AB}. In the limit of $\langle r_A^2 \rangle \to 0$, c_{AB} vanishes as $\langle r_A^2 \rangle$. Thus the sequence

$$\sigma_T^{\rho p} > \sigma_T^{\phi p} > \sigma_T^{\psi p} \qquad (1.4)$$

can be understood semiquantitatively. The rapid decrease is due to the cancellations inherent for a color singlet bound state;

for instance if $\langle r_A^2 \rangle = 0$ (a point-like bound state) and we consider the valence-$q\bar{q}$ Fock state of a meson, then the gluon attachment to the $\bar{q}$ yields an exactly equal but opposite sign contribution compared to that from the attachment to the q. (This is why there is no Pomeron in two-dimensional QCD.[9]) Note that the diagrams for mechanism (c) (and (d)) involving a valence quark from state A are not expected to yield this color cancelation effect; this is an argument against mechanism (c) (and (d)).

Of course it is not necessarily legitimate to restrict ourselves to the exchange of a single quark or single gluon between the Fock states of A and B — multiple exchanges are possible. Multiple exchanges preserve the color singlet cancellation responsible for the size effect; indeed this cancellation guarantees that an infrared finite leading-log perturbative calculation of multiple gluon exchanges can be carried out. (This does not mean that there are no non-perturbative effects which we cannot calculate this way.) However, multiple exchanges generally violate quark counting. In addition the color structure of the final state becomes so complicated that no one has attempted to calculate particle production in such a case. Thus we will restrict ourselves to single quark or single gluon exchange.

Finally, or course, these perturbative QCD models ignore the possible importance of unanticipated non-perturbative effects inherent in the confinement of the quarks within the bound states. Such effects cannot necessarily be factored away from the dynamics as they can be in the short distance physics realm.

The existing QCD based models all fit into the simple pictures of Fig. 1 and Fig. 2 in which multiple exchanges and non-perturbative effects are ignored. We will see that these simple models allow us to understand qualitatively and, in some cases, quantitatively the structure of multiparticle production in the final state of hadronic collisions. Multiparticle production will be presumed to occur as a result of the separation of color and the consequent gluon radiation[10,11,12] or breaking apart of the stretching color flux tubes joining the two or more separating colors.[13] Each of the QCD models has its difficulties and successes. The valence-sea exchange model of Figs. 1(c) and 2(c) suffers moderately severe difficulties in the fragmentation region and, as discussed, lacks the color size effect; this will lead us to favor models based on Fig. 1(a)-(b) or Fig. 2(a)-(b).

B) Dual Pomeron Diagram Model[3,4,5]

The perturbative color exchange model approaches to multiparticle production are different from the dual model approaches in the literature. A convenient visualization of the dual model Pomeron for $\pi\pi$ collisions is shown in Fig. 3(a). One way to think about this picture is to imagine that the color flux tubes

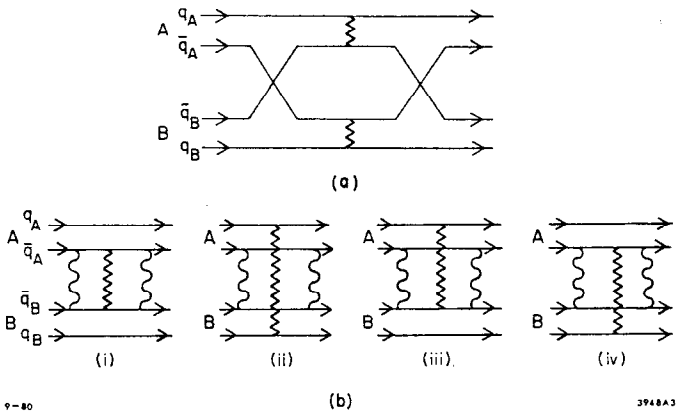

Fig. 3. The squared amplitudes for: a) The dual model Pomeron with multiparticle production indicated by $\lesssim$. b) The gluon exchange "Pomeron".[1] The final state gluon radiation diagrams which typically dominate in lowest order (in the Feynman gauge of the radiated gluon) are drawn. The radiated gluon (and associated multiparticle production) is indicated by $\lesssim$.

which connect q_A - $\bar{q}_A$ and q_B - $\bar{q}_B$ become confused at the moment of interaction and afterwards attempt to connect q_A - $\bar{q}_B$ and $\bar{q}_A$ - q_B, (The colors of q_A and q_B must be the same for this to occur.) Since q_A and $\bar{q}_B$ (and $\bar{q}_A$ and q_B) are moving in opposite directions the flux tubes are stretched and multiparticle production takes place in these two color singlet channels. The Pomeron arises, through unitarity, as a reflection of this multiparticle production.

Several points of comparison with the QCD approaches are noteworthy. First there is no underlying elementary spin 1 particle exchange acting as a perturbative source of the constant total cross section; in particular, no color exchange takes place and there is no obvious mechanism for explaining the strong decrease of σ_T with decreasing beam hadron size. The purely

geometric effect (crudely $\sigma_T \propto (r_A + r_B)^2$) is not sufficient. However, quark counting is natural in the dual model approach.[5] The greatest distinction is in the visualization of final state particle production. In Fig. 3(b) we compare the picture of Fig. 3(a) to that appropriate for gluon exchange. The basic idea is the same as in the dual model picture; separating color charges radiate gluons or break the color string connecting them; this produces hadrons, eventually, as in e^+e^- annihilation. However, the radiation pattern is completely different in general. To see this consider lowest order single gluon radiation in the final state. In Feynman gauge for the radiated gluon all four diagrams of Fig. 3(b) contribute significantly. Only if we require that the radiating subsystem be in a color singlet do we obtain a picture analogous to Fig. 3(a); using this restriction would imply that particle production in the "channels" $q_A - \bar{q}_B$ and $q_B - \bar{q}_A$ is possible but not in the $q_A - q_B$ and $\bar{q}_A - \bar{q}_B$ "channels". This, however, is not a gauge invariant prescription. In a radiation gauge one would obtain an entirely different radiation pattern than in Feynman gauge if only diagrams (iii) and (iv) are kept. Only a full set of diagrams, including still other diagrams than those shown in Fig. 3(b), yields a gauge invariant answer.

This difference is directly related to the fact that in the dual model picture, Fig. 3a, there is no actual color exchange between the colliding mesons as they pass one another. In the perturbative approach (i.e., imagine that the exchange "gluons" of Fig. 3(b) are color singlets) there would be no final state radiation of gluons and hence, little or no particle production. The diagrams i) and ii) would cancel the diagrams iii) and iv), in Feynman gauge, due to the opposite sign coupling of the radiated gluon or color flux tube to the quark compared to the antiquark of the singlet meson. Retaining only $q_A - \bar{q}_B$ and $\bar{q}_A - q_B$ radiation would yield a completely wrong result. I have not seen an explanation in the literature of why the color structure of the dual model Pomeron is that illustrated in Fig. 3(a). Nonetheless, I will discuss in what follows the approach based upon assuming that multiplicity is produced only in the $q_A - \bar{q}_B$ and $\bar{q}_A - q_B$ subsystems and that this multiplicity or radiation is like that in e^+e^- annihilation resulting from $q\bar{q}$ color separation.

II. Multiplicities and Rapidity Distributions

A) Comparison of QCD Exchange Models

We have already referred to the idea that in a QCD based approach to multiparticle production in the final state of a hadron-hadron collision the final particles are produced in response to color separation in the final state just as in e^+e^- annihilation. In the gluon exchange model of Fig. 1(a) the "meson" states after gluon exchange are no longer color singlets and can be expected to "radiate" gluons which in turn create $q\bar{q}$ pairs or gluon pairs through the standard branching processes of QCD.[10,11,12] Ultimately these radiation products match together to form the final hadrons. An altenative picture is that the color flux tube joining the separating colored objects breaks apart, as it is stretched, and in so doing produces the observed final state particles.[13] We will use the radiation language in much of what follows; the color structure of the two approaches is the same. (These approaches are completely different from the older multiperipheral approach in which the final particles are produced virtually over a long time prior to the actual collision.) Exactly how much radiation or particle production takes place and how the radiated particles are distributed is controlled by the relative motion of the "initial" colored particles in the final state. To illustrate the possibilities we will focus on Figs. 1(a) and 1(b).

Let us focus for a moment on the "initial" final state, derived from Fig. 1(a), in which color octet versions of the incoming hadrons' valence states are rapidly separating with essentially the full collision energy. In the center-of-mass the forward and backward moving octet states each have momentum $\sqrt{s}/2$. However, this net momentum need not be equally distributed among the particles comprising the octet jet. To illuminate the possibilities it is useful to consider[14] in detail the lowest order radiation of a gluon in the final state of Fig. 1(a). The diagrams are shown in Fig. 4 where we have squared the amplitudes and shown the radiated gluon. A factor of two is indicated when there are two possible final state "cuts" to be made; this factor occurs whenever a gluon is emitted from one particle and absorbed by another. One can calculate the radiation in either the Feynman gauge or a radiation (transverse)

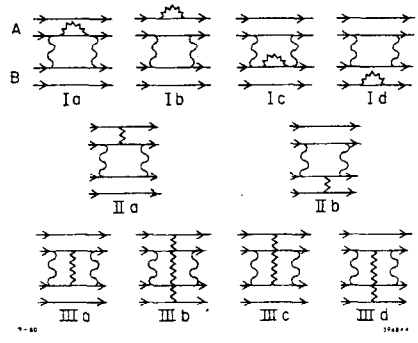

Fig. 4. Lowest order gluon radiation in the final state of a gluon exchange collision of two pions. The radiation gluon is indicated by the angular zig-zag line.

gauge. The various diagrams enter differently in the two gauges. Diagrams of class I and II are generally most important in the radiation gauge while diagrams of class III generally dominate in Feynman gauge. Denoting the photon energy by k and its rapidity by y ($y = 1/2\ \ell n[(1+\cos\theta)/(1-\cos\theta)]$) we obtain in either gauge the following results for the gluon multiplicity distribution dn/dkdy. Consider two extremes:

i) The momentum of A (p_A) is shared equally by the constituent quark and antiquark (and similarly for B). Then

$$\frac{dn}{dkdy} \propto \frac{12}{k} \begin{cases} y_{max} = \ell n(p_A/m) \\ y_{min} = \ell n(p_B/m) \end{cases} \qquad (2.1)$$

(m = quark mass) regardless of whether the interacting constituents are quarks or antiquarks.

ii) The momenta of the interacting quarks and/or antiquarks (one in A and one in B) are both much smaller than their mass. Then

$$\frac{dn}{dkdy} \propto \begin{cases} \frac{16}{3}\frac{1}{k} - 2\frac{1}{k}\frac{1}{\cosh^2 y} & \text{gluon exchange between q-q or } \bar{q}\text{-}\bar{q} \\ \frac{16}{3}\frac{1}{k} - \frac{1}{3}\frac{1}{k}\frac{1}{\cosh^2 y} & \text{gluon exchange between q-}\bar{q} \end{cases} \qquad (2.2)$$

with $y_{max} = \ell n(2p_A/m)$, $y_{min} = \ell n(2p_B/m)$.

Several features of the results are noteworthy.

1) If the quarks in the octet versions of the incoming bound states are both fast moving one obtains radiation which is indistinguishable from that of coherently moving octets. (Even the y_{max} and y_{min} are the same if the octets have the same momenta p_A and p_B and have mass = $2m_{quark}$.) This similarity to octet radiation holds even if the constituent quarks do not share

equally p_A (or p_B) so long as their fraction of the big momentum p_A (or p_B) is significant.

2) If the scattering quarks have momenta significantly less than their masses, the radiation consists of a piece which is the same as radiation between a 3 and $\bar{3}$ of color moving with p_A and p_B respectively (i.e., the same as we find in e^+e^- annihilation) and a negative contribution which is important in the central region, $y \approx 0$.

In all cases the dominant contribution yields a flat rapidity plateau with height given by $\int_{k_{min}}^{k_{max}}(dk/k)$. The lower limit of this integral is, of course, set by bound state sizes through the hadronization process in the final state. The upper limit is not well determined. One can obtain a gauge invariant calculation only if k_{max} is the same for every graph in Fig. 4. The only consistent choices are to take k_{max} as either a fixed number determined by the incoming bound states or as being some fraction of the total available center-of-mass energy, $W = \sqrt{s}$. The latter choice leads to a rising plateau at any fixed value of y. A rising plateau is observed in e^+e^- annihilation where the color configuration is sufficiently simple that only $k_{max} \propto W$ could lead to the rising plateau. We will make this choice; further discussion will occur shortly. One then finds in all cases

$$\left.\frac{dn}{dy}\right|_{y=0} \propto \ell n\ W \tag{2.3}$$

and

$$\langle n \rangle \propto a\ \ell n^2\ W + b\ \ell n\ W + c \tag{2.4}$$

In computing $\langle n \rangle$ the $1/\cosh^2 y$ terms, present when the initiating gluon exchange is between slow quarks, contribute only to the $\ell n\ W$ term and would be hard to detect. On the other hand at $y \approx 0$ they lead to the following comparison.

$$\left.\frac{dn}{dy}\right|_{y=0} \propto \ell n\ W \begin{cases} 12 & \text{gluon exchange between fast quarks} \\ \frac{16}{3} & e^+e^- \text{annihilation or fast separating } 3\text{-}\bar{3} \text{ in general} \\ \frac{15}{3} & \text{gluon exchange between a slow } q_A \text{ and slow } \bar{q}_B \text{ or vice versa} \\ \frac{10}{3} & \text{gluon exchange between a slow } q_A \text{ and a slow } q_B \text{ or } \bar{q}_A \text{ and } \bar{q}_B \end{cases} \tag{2.5}$$

Thus for pp collisions via gluon exchange the central plateau height could be 9/4 as high as that in e^+e^- annihilation if the interacting quarks are fast or 5/8 as high if the interacting quarks are slow.

In considering Fig. 1(b) we examine the cases:

1) The momenta of q' and $\bar{q}'$, the quarks left over from the gluon bremstrahlungs are smaller than their masses. This is the natural case since a constant total cross section is obtained only if at least one of the bremstrahlung gluons is soft. Then

$$\frac{dn}{dkdy} \propto \frac{12}{k} - \frac{21}{8}\ \frac{1}{k}\ \frac{1}{\cosh^2 y} \tag{2.6}$$

The large y region is like that for separating octets; but at $y \approx 0$ the plateau height is smaller than for separating octets.

2) The momenta of q' and $\bar{q}'$ are both a significant fraction of the respective bound state momenta — that is the triplet "jets", are in each case moving together more or less coherently. Not surprisingly the radiation is exactly that of separating color triplet states,

$$\frac{dn}{dkdy} \propto \frac{16}{3}\ \frac{1}{k} \tag{2.7}$$

with y_{max} and y_{min} determined by details of momenta fractions and masses. This configuration probably requires that q' and $\bar{q}'$ reinteract with the other members of their corresponding colored spectator jets in order to be speeded up from their initially small momenta imparted by the soft gluon bremstrahlung. This coherent triplet picture will present difficulties when we consider fragmentation distributions.

The central plateau heights are given below.

$$\left.\frac{dn}{dy}\right|_{y=0} \propto \ell n\, W \begin{cases} \frac{75}{8} & \text{slow q' and } \bar{q}' \\ \frac{16}{3} & \text{fast q' and } \bar{q}' \end{cases} \tag{2.8}$$

All of the above results for Fig. 1(a) and 1(b) are somewhat modified if we consider the higher Fock state pictures, Fig. 2(a)-(b), where the gluon which initiates the collision attaches to a gluon Fock state component. This will be discussed further later.

B) Constraints from the Data

What does the data say? Two types of information are available which bear on the above type of predictions; these are the average charged particle multiplicity and the central plateau height. The data clearly shows that $\langle n \rangle_{e^+e^-} \gtrsim \langle n \rangle_{pp}$. Gluon exchange between fast quarks leaving effectively octet jets radiating in the final state would predict the opposite, as would quark exchange with slow q' and $\bar{q}'$. Thus we are left with the two second type possibilities. The data[15] are shown in Fig. 5,

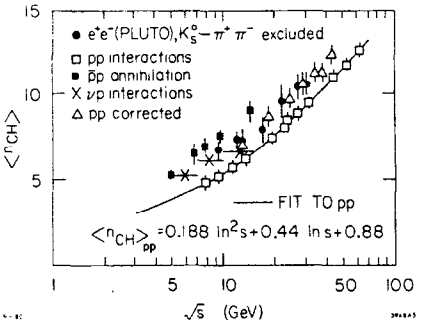

Fig. 5. Charged multiplicities in various types of reactions as a function of the total energy available for hadron production, $W = \sqrt{s}$.

where the PLUTO data for e^+e^- annihilation $\langle n_{charged} \rangle$ are compared to those for pp, $\bar{p}p$ and πp collisions. Only the PLUTO data have been plotted since, at the time of writing, it was the only group to have corrected for $K^0_S \to \pi^+\pi^-$ decays[15] —— it is essential to plot only primary charmed quark multiplicities when comparing to data controlled by up and down quark radiation. The correction results in an average decrease of about .7 units in $\langle n_{ch} \rangle$, Also shown on the graph is a fit to pp scattering multiplicities corresponding to the form

$$\langle n_{ch} \rangle = a' \ell n^2 s + b' \ell n s + c' \qquad (2.9)$$

predicted as discussed on the basis of QED-like gluon radiation from separating color charges. More recently QCD calculations,[12] which include the gluon branching allowed by the three gluon coupling, have suggested a form in e^+e^- reactions

$$\langle n_{ch} \rangle = a + b \exp \left[c \sqrt{\ell n \, s/\Lambda^2} \right] \qquad (2.10)$$

which provides an equally good fit to either e^+e^- or pp multiplicity data; its use in pp reactions is not, however, perturbatively justified.[16]

Several cautions are necessary, however, in making a direct comparison between e^+e^- and other final states. First it should

be noted that, whereas e^+e^- annihilation need not have any baryons in the final state, pp collisions require two baryons in the final state and νp one. At least one attempt[17] has been made to correct for this effect; the procedure is to look at one hemisphere of a pp collision, measure the energy of the fastest proton in that hemisphere and define the available energy for remaining hadron production as

$$E_{had} \equiv E_{beam} - E_{fastest\ proton} \tag{2.11}$$

The multiplicity remaining in the one hemisphere is doubled and compared to e^+e^- data at

$$2E_{had} = \sqrt{s_{e^+e^-}} \tag{2.12}$$

These points are plotted in Fig. 5 as the pp-corrected points. Obviously there is considerable similarity between e^+e^- and pp-corrected $\langle n_{ch} \rangle$ data. A similar analysis in νp scattering would be highly desireable.

Returning to our discussion of models it is amusing to note that the simplest explanation of the similarity between e^+e^- and pp-corrected data would be to suppose that a picture such as Fig. 6(c) (in which a baryon fragment is added to a picture of the mechanism Fig. 1(c) type) was controlling multiplicity production in the presence of a leading proton rather than Fig. 6(a) based on Fig. 1(a) (gluon exchange). In Fig. 6(c) the remaining particle production in the leading proton hemisphere is controlled by quark-color triplet radiation, assuming q' is fast, and should be closely related to

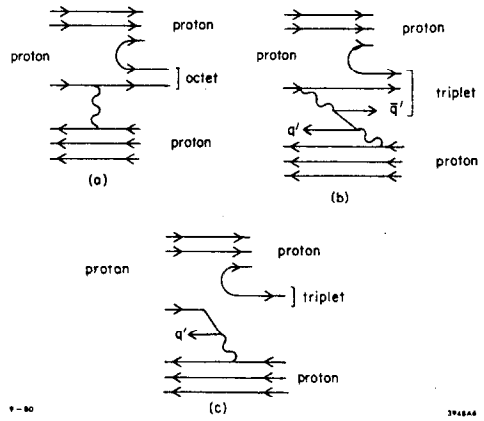

Fig. 6. Final states appropriate to fast baryon production in pp collisions following: a) gluon exchange; b) "sea" quark exchange; and c) sea quark absorption by a valence quark.

e^+e^- particle production. This should be compared to Fig. 6(a) in which a quark and antiquark in an octet state remain in the same hemisphere as the leading proton and similarity to radiation in e^+e^- annihilation requires that the quark interacting with the gluon be slow; the quark-antiquark octet state cannot radiate as a coherent unit because it would do so with an effective octet color "charge" which is higher than the triplet "charge" appropriate to the e^+e^- annihilation final state. However, as discussed with regard to the mechanism of Fig. 1(c), the picture in Fig. 6(c) leads to forward-backward correlations in fragmentation which are not observed. Fig. 6(b) (analogous to Fig. 1(b) could also lead to e^+e^--like color triplet radiation provided all the quarks in the spectator triplets act coherently, i.e., q' and $\bar{q}'$ are fast. Unfortunately, as discussed in Sect. III, in this same coherent approximation the backward and forward fragmentation distributions fail to factorize, in disagreement with experiment.

Thus a seemingly simple experimental result requires a rather sophisticated explanation. In the octet gluon-exchange model which agrees with the factorization and fragmentation distributions (Sect. III) the interacting quark of the final state octet jets must be very slow moving.

A similar experimental observation to that discussed above is that[18,19]

$$\langle n\rangle_{\pi p} = \frac{1}{2}\langle n\rangle_{e^+e^-} + \frac{1}{2}\langle n\rangle_{pp} \tag{2.13}$$

all evaluated at the same W. This suggests that one of the pion's valence state quarks is absorbed by the collision with the proton target (analogously to Fig. 1(c)) leaving a jet in the forward direction consisting of just a single quark as in e^+e^- annihilation. Once again this picture predicts a violation of factorization for the forward backward fragmentation distributions. A πp mechanism analogous to that shown in Fig. 1(b) with q' and $\bar{q}'$ fast would also yield the above type of formula, but this mechanism will be shown to disagree with fragmentation distributions in Sect. III. The only way to understand the fragmentation results is in terms of the gluon exchange approach, Fig. 1(a). The above multiplicity result requires in the context of this mechanism that the interacting quarks in the pion and proton Fock states be very slow.

A more direct test of models is to look directly at dn/dy at $y = 0$. This is done in Fig. 7(a). The only available high energy e^+e^- data is that from TASSO[20] and is uncorrected for $K^o_S \to \pi^+\pi^-$. (In addition the raw (i.e., uncorrected) TASSO data for $\langle n_{ch} \rangle$ appears to be above that from PLUTO and JADE.)

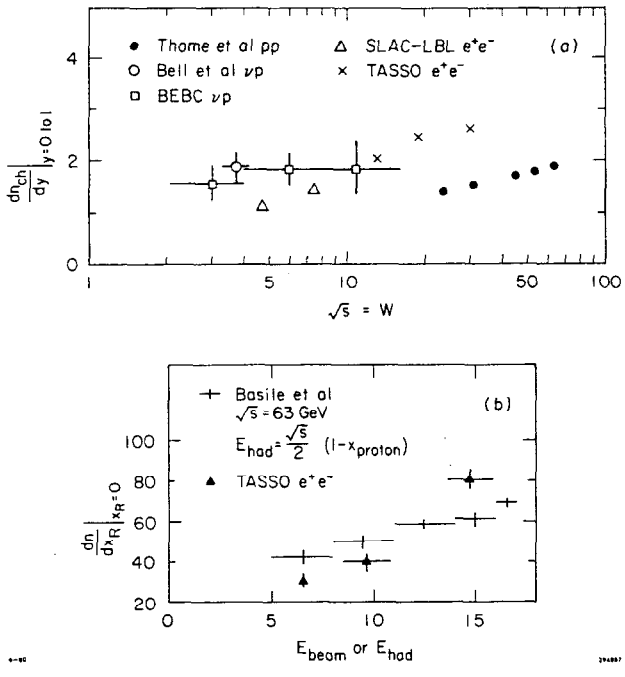

Fig. 7. a) Plot of $(dn/dy)|_{y=0}$, for various types of reactions[20,21,22] as a function of W. b) Plot of dn/dx_R at $x_R=0$ for pp-corrected and TASSO distributions;[17] x_R is defined as $x_R = p/E_{had}$ and $x_R = p/E_{beam}$, respectively.

Nonetheless, it seems clear that the plateau in e^+e^- annihilation is higher than in pp collisions[21] at the same $\sqrt{s}$. This effect is reduced in size but still present even when one does the leading proton subtraction.[17] This is illustrated in Fig. 7(b) where we plot dn/dx_R at $x_R = 0$ versus E_{beam} $(=E_{had})$. The TASSO data rises more rapidly than the corrected pp points. If this persists after correction for $K^o_S \to \pi^+\pi^-$ it is clear that models derived from Fig. 1(b) type diagrams with q' and $\bar{q}'$ fast moving, so that the final state consists of radiating triplets of color, are in difficulty. A direct extraction of the dn/dy distribution in the pp-corrected case would be very helpful.

If dn/dy for the pp-corrected data persists in being lower than that seen in e^+e^- annihilation at the same E_{had} value, then the simple explanations of the $\langle n \rangle$ similarity based on Fig. 6(b) or 6(c) are clearly wrong.

The observant reader will note immediately that the ratio

$$\left[dn^{pp}/dy\right]_{y=0} \Big/ \left[dn^{e^+e^-}/dy\right]_{y=0} = \frac{5}{8} \qquad (2.14)$$

predicted for gluon exchange between slow quarks actually describes the raw $(dn/dy)|_{y=0}$ data of Fig. 7(a) quite reasonably.

Thus we seem to be led by a combination of experiment and theory to consider in pp collisions the gluon exchange picture analogous to Fig. 1(a) in which the final state octet proton jets divide themselves into a slow moving triplet quark and a fast moving antitriplet diquark (plus possible gluons); each component radiates independently according to the discussion given earlier. This picture comes close to describing the $\langle n \rangle$ and dn/dy data. A particularly revealing prediction is that of a dip in dn/dy in the y near zero region once the plateau has expanded enough to reveal a $1/\cosh^2 y$ term (see Eq. (2.2)). Such a dip does appear to be developing in the Thome et al data,[21] Fig. 8. In contrast the e^+e^- annihilation data should not develop a pronounced dip. In general, if a plateau does not show any structure as a function of y it is an indication that all the colored objects that form a given final state jet are moving with approximately the same speed. We will see another example of this when we discuss the dual model approaches.

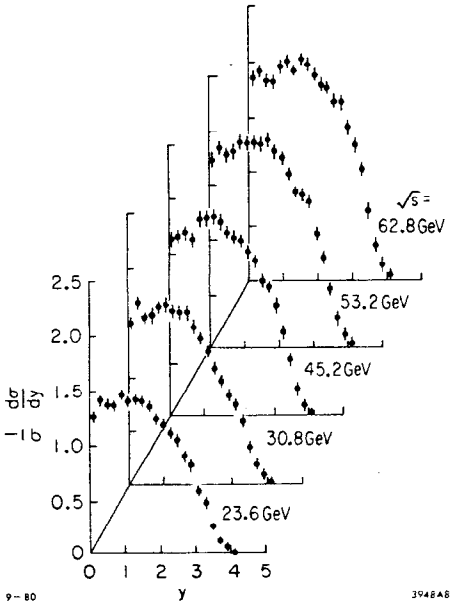

Fig. 8. The dn/dy plots of Thome et al[21] at various center-of-mass energies

C. Universality of the Particle Production Mechanism — Constraints from Deep Inelastic Scattering.

Before proceeding further, I would like to return to the most important assumption underlying the preceding predictions. This regards the amount of color radiation or multiplicity production in a situation like e^+e^- annihilation, where the created q and $\bar{q}$ have the ability to be far off-shell, as compared to hadron-hadron collisions, where the final state quarks could conceivably be restrained from being far off-shell by the bound state wavefunction. In a naive radiation approach this off-shellness determines the upper limit, k_{max}, on the integral $\int dk/k$. It is this upper limit which determines the plateau height. In the preceding we assumed that k_{max} grows as the total available energy in the system of separating color, $k_{max} = fW$. In the naive radiation approach this requires that the exchange gluon, which establishes the initial color separation, carry a non-vanishing longitudinal momentum;[23] even if the initial bound state quarks are on-shell this allows the final radiating quarks to be off-shell. While there is nothing to disallow this it may be that this type of detail is taking the radiation model too seriously. Even if we have on-shell separating colored systems it is clear that the gluon binding "string" or flux tube which joins them is being stretched and will break by creating $q\bar{q}$ pairs. The number of such pairs is certainly proportional to the "charge" of the separating colored objects and is most naturally controlled by the amount of energy available for stretching the "string". This non-perturbative picture would, thus, also predict that the plateau height is a function only of the available energy W of the separating colored systems, and that this function should be universal — independent of the reaction establishing the color separation. In the radiation terminology, the fraction f should be reaction independent.

Fortunately experiment provides us with at least one testing ground for these ideas. This is deep inelastic scattering, e.g., νp scattering illustrated in Fig. 9. Here the quark struck by the W^+ has the ability to be far off-shell prior to radiating (its off-shellness is generally a function of both W^2 and Q^2) whereas the

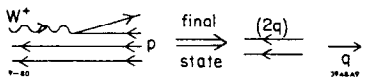

Fig. 9. Deep inelastic νp scattering in the W^+p center-of-mass frame.

diquark system (which includes, in general, possible gluons and $q\bar{q}$ pairs) is constrained by the bound state wavefunction to be essentially on-shell. As is well known this off-shell ability of the forward going quark ($x_F > 0$) results in a rise in $\langle p_T^2 \rangle$ for $x_F > 0$ as W^2 and Q^2 increase, whereas $\langle p_T^2 \rangle$ for $x_F < 0$ is much more slowly varying,[24] Fig. 10(a). In contrast the forward and backward multiplicities do not seem to exhibit such a marked difference,[24] Fig. 10(b). Instead they rise at about the same rate

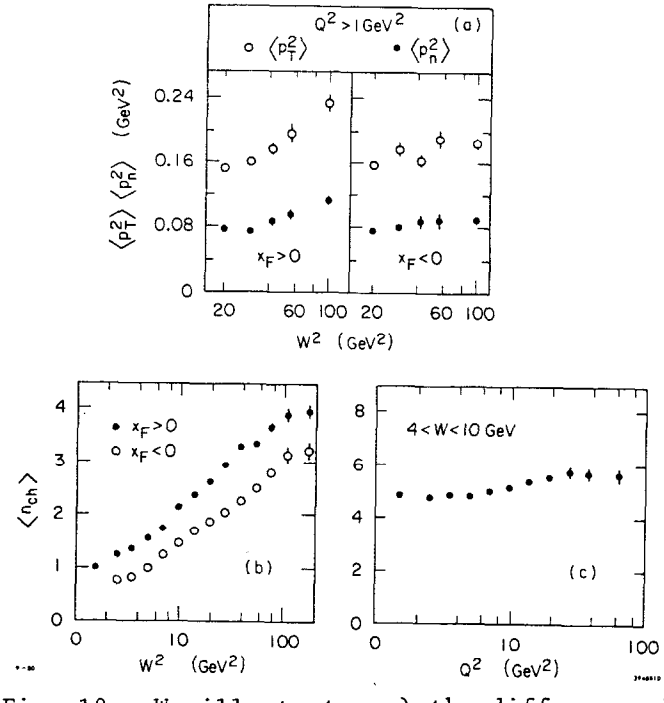

Fig. 10. We illustrate: a) the difference in $\langle p_T^2 \rangle$ in the forward and backward hemispheres of a 2p collision; b) the similarity of $\langle n_{ch} \rangle$ in the $x_F > 0$ and $x_F < 0$ hemispheres; and c) the very weak dependence of $\langle n_{ch} \rangle$ on Q^2 at fixed W^2.

with W^2, the fixed finite difference undoubtedly attributable to the requirement that a baryon appear in the $x_F < 0$ region. More importantly the plateau heights in the $x_F < 0$ and $x_F > 0$ target and current regions are the same[22] and the average multiplicity and common plateau height are essentially independent of Q^2 at fixed W^2, despite the difference in the off-shell ability of the forward and backward systems. This is illustrated in Fig. 10(c).

Finally, the common plateau height[22] is approximately the same as that seen in e^+e^- annihilation at the same W (see Fig. 7) implying that the plateau height as a function of W is a universal function, independent of reaction — in the radiation model the fraction f is reaction independent. (Note that the separating colors are the same in the two reactions.) Note also that the complexity of the diquark system does not influence the produced multiplicity — as Q^2 decreases at fixed W^2, x_{Bj} decreases, the $q\bar{q}$ "sea" component of the proton becomes more important, but the produced multiplicity is unaltered at fixed W^2. "Radiation" and resulting multiplicity are determined only by the color structure and available energy, W, in the final state.

D) Comparisons between πp, $\bar{p}p$ and pp

Turning for a moment to πp and $\bar{p}p$ reactions let us ask what the possibilities analogous to those considered in pp scattering would predict. If we employ gluon exchange and all final state jet quarks are fast moving there would be little difference between $\bar{p}p$, πp and pp predictions. In particular all dn/dy's would be the same at y = 0 (and 9/4 the dn/dy of e^+e^- annihilation[10]) for the same available energy W. If the quarks which interact with the gluon are very slow then we predict that the $\ell n^2 W$ terms in $\langle n \rangle$ for πp, $\bar{p}p$ and pp should all be the same but that the $\ell n\, W$ terms would be different due to the differences in dn/dy at y = 0. Counting the number of qq or $\overline{qq}$ vs $q\bar{q}$ interactions in the various cases we obtain from Eq. (2.2)

$$\left[\frac{dn^{\bar{p}p}}{dy} : \frac{dn^{\pi p}}{dy} : \frac{dn^{pp}}{dy}\right]_{y=0} = \frac{15}{3} : \frac{12.5}{3} : \frac{10}{3} \qquad (2.15)$$

There is some experimental evidence[25] for such differences; even the numerical factors are about correct.

One may ask in the slow interacting quark approach whether the difference in $\bar{p}p$, πp and pp plateau heights, as well as the smaller plateau height of, for example, pp relative to e^+e^-, should persist as the energy W increases beyond that presently available. The answer is model dependent. If the interacting quarks' momenta which are small at current W values become significantly bigger (as W increases) than their masses, then the picture would change completely; $\bar{p}p$, πp and pp plateau

heights all would become equal and 9/4 as high as the e^+e^- plateau height.[10]

A legitimate question to ask is why the interacting quark should be expected to be slow. In general, it can be slow only if it has lost energy by gluon emission prior to the interaction. Thus the spectator system to the interaction must include gluons. These do not affect the total amount and distribution of radiation provided they are energetic. At present, however, there is no perturbative QCD argument that requires the softness of the interacting quark. Within the dual model approaches Regge theory predicts that the interacting quark should be soft and, as in the QCD model, this softness will be crucial to the phenomenological successes of the approach. Without further ado let us turn to the dual model picture.

E) The Dual Model Picture[3,4,5,26]

i) pp Collisions

As reviewed in Sect. I, the QCD approach to multiplicities is rather different in spirit to that based on the dual Pomeron picture. To recall, the dual Pomeron approach views final state multiplicities as arising via the superposition of two color singlet $3\text{-}\bar{3}$ radiation channels. In this case it is most appropriate to assume that it is the subenergy of each channel that determines the plateau height for that channel. Thus in pp collisions we have the final state picture of Fig. 11(a). For πp collisions the picture is Fig. 11(b).

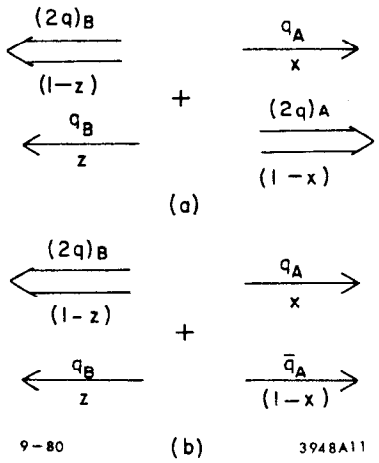

Fig. 11. Dual Pomeron model pictures for: a) the pp final state; and b) the πp final state. The momentum fractions of the quarks in the forward and backward moving bound state jets are indicated by x and z, respectively.

In pp collisions we superimpose two deep inelastic (2q)-q type multiplicity patterns which, as we have seen, are the same as the $q\text{-}\bar{q}$ multiplicity pattern when $W^2_{2q\text{-}q} = W^2_{q\text{-}\bar{q}}$. The subenergies $W_{(2q)_B\text{-}q_A}$ and $W_{(2q)_A\text{-}q_B}$ are determined by the momentum distribution between quark and diquark in the incoming protons. A rough picture of dn/dy is given in

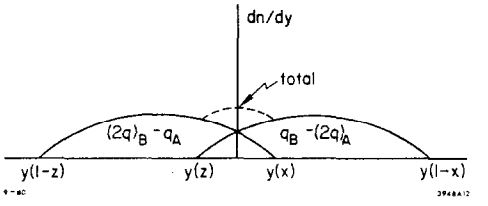

Fig. 12. A rough picture of the superposition of the two 2q-q plateaus. The rapidities of the source quarks and diquarks corresponding to Fig. 11 are shown.

Fig. 12. To obtain a reasonable plateau height, $(dn/dy)_{pp} < (dn/dy)_{e^+e^-}$, it is necessary that the diquark carry significantly more momentum on the average than the quark. This has two effects: 1) the plateaus are then not centered on the origin and their overlap is reduced, and 2) the subenergies and hence the plateau heights in each 2q-q channel are smaller than if the full W^2 determined the plateau heights of each channel. Thus

$$\left.\frac{dn^{pp}}{dy}\right|_{W^2} < 2 \left.\frac{dn^{q-2q}}{dy}\right|_{W^2 \langle x(1-z)\rangle} . \qquad (2.16)$$

Of course as W increases larger portions of the two plateaus overlap and the inequality becomes an equality. This would cause a rise in the pp plateau height even if the e^+e^- plateau height were roughly energy independent. Including the observed rise in the e^+e^- plateau leads us to expect a very rapid rise in the pp plateau height at energies above those currently available; eventually the pp plateau height should be twice the e^+e^- plateau height at the appropriate reduced W.

Exactly how asymmetric the quark and diquark momenta are and how much energy is required to reach the asymptotic situation depends on the proton wave function. QCD analyses[27] suggest that in the valence Fock state the distribution is

$$G^V_{q/p}(x) \propto x(1-x)^3 \qquad (2.17)$$

The average value of x and other quantities would then be

$$\langle x \rangle = \frac{1}{3}$$

$$\langle 1 - z \rangle = \frac{2}{3}$$

$$\langle W^2 \rangle_{q-2q} = W^2 \langle x(1-z) \rangle = \frac{2}{9} W^2 \quad . \qquad (2.18)$$

By reference to Fig. 7 we see that for $20 < W < 60$ each q-2q plateau would have a height generally bigger than the pp plateau height. Even accounting for the lack of centering, it is not possible to make the superposition agree with the data.

What has been done to achieve agreement is to take[5]

$$G^R_{q/p} \propto \frac{1}{\sqrt{x}} (1 - x)^3 \tag{2.19}$$

i.e., to use a Regge-like form for the distribution function. As mentioned earlier the dual model picture suggests such a form and in QCD it could arise from the effects of radiating gluons from the interacting quarks prior to the collision. Let us examine the consequences of Eq. (2.19). We find

$$\langle x \rangle = \frac{1}{9}$$

$$\langle 1 - z \rangle = \frac{8}{9}$$

$$\langle W^2 \rangle_{q\text{-}2q} = \frac{8}{81} W^2 \tag{2.20}$$

Now the typical single q-2q plateau height (read off of the e^+e^- results) is roughly equal to the pp plateau height and the lack of overlap is much more extreme. Consistency is obtained in an "accidental" fashion. For numerical details see some of the other contributions to this conference.

ii) πp Collisions

In πp collisions the use of the Regge form of G(x) becomes even more crucial. For a valence Fock state QCD predicts a symmetric distribution such as

$$G^V_{q/\pi}(x) \sim x(1 - x) \tag{2.21}$$

whereas a Regge form would be

$$G^R_{q/\pi} \sim \frac{1}{\sqrt{x}} (1 - x) \tag{2.22}$$

Combining the valence forms of $G_{q/p}$ and $G_{q/\pi}$ yields a superposition of the type shown in Fig. 13(a) (see Fig. 11(b)). This yields far too much overlap of the q-2q and $q\bar{q}$ plateaus and too high a πp plateau height as well as a rather asymmetric dn/dy distribution. Employing Regge forms for the proton and pion wavefunctions creates the situation shown in Fig. 13(b) in which

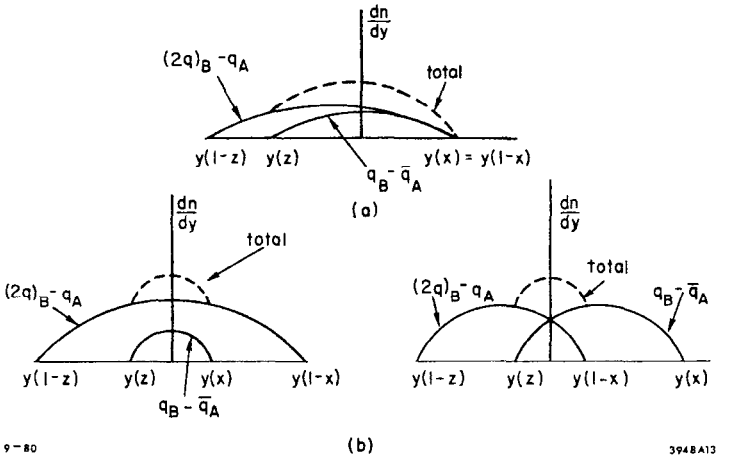

Fig. 13. Plateau pictures for πp collisions employing: a) valence distributions; and b) Regge distributions. In b) we must actually take the average of the pictures shown; in one $\bar{q}_A$ is Regge behaved — in the other, q_A.

we average the results for a slowed-down Regge-like quark in the pion and for a slowed antiquark in the pion. This latter picture agrees approximately with experiment when the numerics are put in. One obtains $(dn/dy)_{\pi p} \overset{y=0}{\approx} 1.2(dn/dy)_{pp}$ at $\sqrt{s} = 20$ in agreement with experiment. Asymptotically pp and πp plateaus have equal height. Using the valence forms for the pion and proton distributions would have produced a much larger ratio than seen for πp to pp plateau heights at current energies. For either the valence or Regge forms of the G's

$$\left(\frac{dn}{dy}\right)^{p\bar{p}}_{y=0} \geq \left(\frac{dn}{dy}\right)^{\pi p}_{y=0} \geq \left(\frac{dn}{dy}\right)^{pp}_{y=0} \tag{2.23}$$

with equality asymptotically approached.

Like the gluon exchange models, the above dual Pomeron approach lacks naturalness in its explanation of the experimental similarity of the final multiplicity, when the leading proton is extracted, to that in e^+e^- annihilation at the same E_{had}, as discussed around Eq. (2.11). Extracting a forward leading proton converts the q_B-$(2q)_A$ plateau to a reduced q_B-$\bar{q}'_A$ plateau, see Fig. 14, but does not affect the other $(2q)_B$-q_A plateau. It can only be accidental that the resulting multiplicity is the same as in a $q\bar{q}$ e^+e^- final state at the appropriate E_{had}. There is a

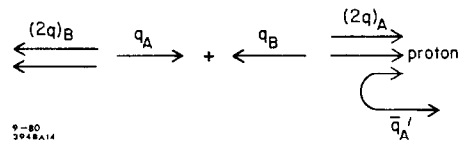

Fig. 14. The dual Pomeron final state in the presence of a leading proton.

similar lack of naturalness in explaining the $\langle n \rangle_{\pi p}$ observation of Eq. (2.13).

F) Points of Difference Between the QCD and Dual Pomeron Models and a Common Problem.

It is worth emphasizing a few points of difference between the phenomenology of the dual Pomeron approach and that of the QCD "radiation" approach. At intermediate energies the pp plateau of the dual Pomeron model is typically characterized by a smoothed-out bump in the y=0 region. Presumably this bump has not appeared at current energies because of the lack of overlap between the two plateaus of Fig. 12 and the fact that an integral over x and z is performed which smooths it out; but as the energy increases it should become apparent. In contrast the QCD "radiation" approach predicts that there should be a dip in the pp plateau in the y=0 region so long as the interacting quarks are slow. If as the energy increases they eventually speed up, this dip should be filled in but a bump should not appear. Similar statements apply to πp and $\bar{p}p$ collisions. Secondly, in both the gluon exchange and dual Pomeron models at very high energies (when, presumably, the interacting quarks are fast in both approaches), the pp plateau height should be twice an appropriate e^+e^- plateau height. However, in the dual Pomeron model the appropriate e^+e^- plateau height to use is that evaluated at the reduced W as in Eq. (2.20) whereas in the gluon exchange QCD "radiation" model the appropriate plateau height should be read off of e^+e^- data at the same total W.

Before ending this section on multiplicity, I would like to return to the point that both the gluon exchange based models and the dual Pomeron models require that the interacting quark be much slower than the remaining spectator system (e.g., the "diquark" system in pp collisions). As already mentioned, the only way to obtain a slow interacting quark in QCD is if the typical Fock state of the colliding hadron is more complicated than the valence state; for example, a quark can slow down by

gluon emission — these gluons then become part of the spectator system. This presents a problem in both approaches. The gluons need not always be part of the spectator system. In the QCD approach the diagrams such as shown in Fig. 2(a)-(c) where the exchange or bremstrahlung gluon initiating the collision interacts with a gluon in the hadron Fock state should also be important.[28] In the dual Pomeron approach there seems to be nothing to prevent a hadron from separating itself into a gluon and an appropriate color octet spectator system. In either case the multiplicity patterns would, in general, be quite different than when a slow quark is controlling the radiation. In the dual model approach one would expect to have collisions in which the final state is a superposition of two color octet type plateaus, Fig. 15, with correspondingly larger plateau heights. The model's agreement with experiment could easily be destroyed. Similar problems, though slightly less severe, arise in the QCD approach. These possible difficulties require further investigation. At the moment the models cannot be regarded as fully self-consistent; we simply assume that only the quark components of the colliding hadrons can be slowed down by the interaction.

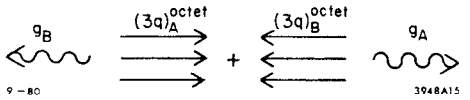

Fig. 15. The final state structure of the dual Pomeron model when the slowed down interacting particle is a gluon.

Finally, I would like to emphasize the great importance of attempting to demonstrate experimentally that radiation from a color octet actually is different from that of a color triplet. The only direct test requires the isolation of a gluon jet. There are a number of experimental situations in e^+e^- annihilation and high-p_T jet production in which this may be possible. If a gluon jet does not produce substantially more multiplicity than a quark jet once its energy is large, then all the final state particle production approaches discussed here will need to be reconsidered.

III. Fragmentation Disturbutions

A) Quark and Diquark Fragmentation

We begin our discussion of fragmentation with a review of experiment and theory for quark and diquark fragmentation functions. A convenient experimental situation in which to examine them is

$$\nu p \to \mu^- h^{\pm} X$$

The best data to date appear to be those from BEBC,[22] Fig. 16. In the $x_F > 0$ region where we have u quark fragmentation the standard result (x_F measures the momentum fraction, x, of the hadron with respect to the u quark.)

$$\frac{dN^{u \to \pi^+}}{dx} \sim (1 - x) \qquad (3.1)$$

is apparent. Data from two other groups is shown in Fig. 17 [22] for $d \to \pi^-$ which confirms this form for favored fragmentation from a quark. The same result is, of course, obtained in e^+e^- annihilation.[30]

In the backward direction one has the fragmentation of a diquark

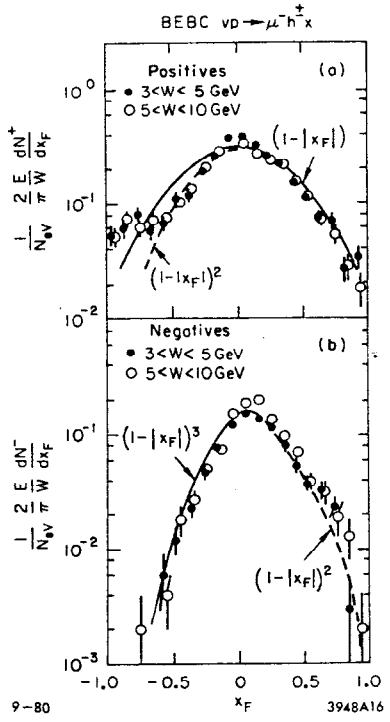

Fig. 16. The distributions of positive and negative hadrons in the current (u quark) and target (2u "diquark") fragmentation regions, $x_F > 0$ and $x_F < 0$, respectively of a νp collision.

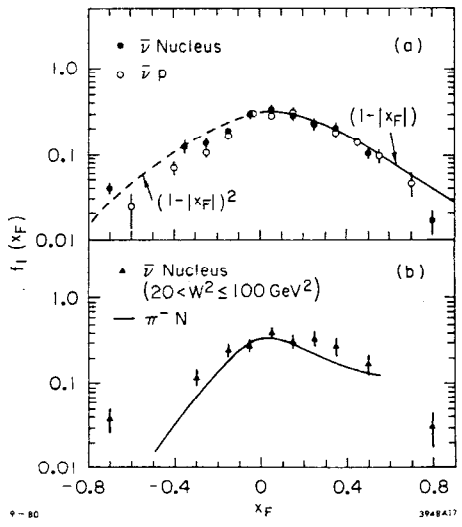

Fig. 17. Lorentz-invariant distributions of negative hadrons in the $x_F > 0$ and $x_F < 0$ d-quark and ud-"diquark" fragmentation regions of a $\bar{\nu}p$ collision. Also shown are corresponding $\bar{\nu}$ nucleus results. These curves are from Ref. 29.

system. From Fig. 16. we obtain

$$\frac{dN}{dx}^{(uu) \to \pi^+} \sim (1 - x)^2 \tag{3.2}$$

Fig. 17 shows a similar result for $(ud) \to \pi^-$. Only the BEBC data allows a determination of unfavored fragmentation. From Fig. 16

$$\frac{dN}{dx}^{u \to \pi^-} \sim (1 - x)^2 \tag{3.3}$$

and

$$\frac{dN}{dx}^{uu \to \pi^-} \sim (1 - x)^3 \tag{3.4}$$

i.e., each is a single power higher than the favored fragmentation powers.

i) Point-Like QCD Fragmentation

Before turning to the hadron collision situation it is worth reviewing our understanding of the above simple results. QCD makes specific predictions in all cases. From Fig. 18(a)

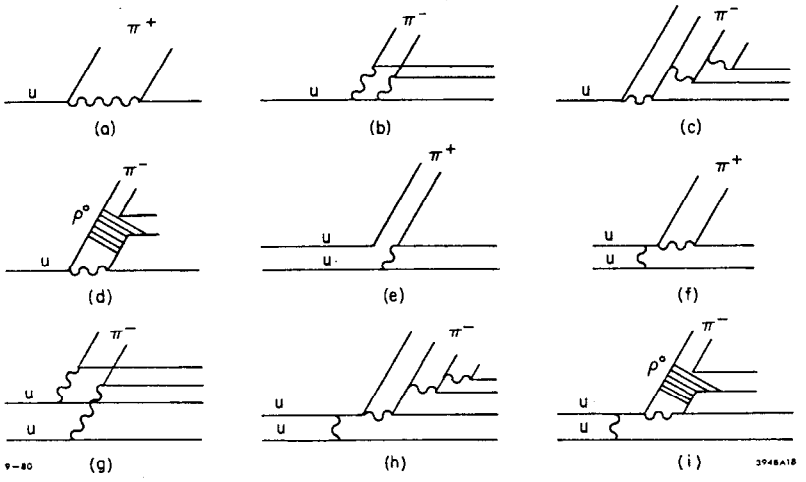

Fig. 18. Various elementary QCD diagrams for:
a) $u \to \pi^+$; b) $u \to \pi^-$; c) $u \to \pi^-$ with only hadronic spectators; d) $u \to \pi^-$ via ρ^0 decay; e) $(uu) \to \pi^+$; f) $(uu) \to \pi^+$ via quark decay; g) $(uu) \to \pi^-$; h) $(uu) \to \pi^-$ with only hadronic spectators; and i) $uu \to \pi^-$ via ρ^0 decay.

we obtain[31] (without including spin effects)

$$\frac{dN^{u \to \pi^+}}{dx} \underset{x \to 1}{\sim} (1 - x) \quad . \tag{3.5}$$

Including spin yields an approximately similar form[32]

$$\frac{dN^{u \to \pi^+}}{dx} \underset{x \to 1}{\sim} (1 - x)^2 + \text{const.} \tag{3.6}$$

Fig. 18(b), the most elementary QCD diagram for a disfavored quark fragmentation,[34] yields, in the spinless approximation,

$$\frac{dN^{u \to \pi^-}}{dx} \underset{x \to 1}{\sim} (1 - x)^2 \quad . \tag{3.7}$$

The result including spin has not yet been computed. These two point-like QCD predictions are in substantial agreement with experiment. They can be summarized in terms of the counting rule[33,34]

$$\frac{dN}{dx} \sim (1 - x)^{2n_H + n_{PL} - 1} \tag{3.8}$$

where n_{PL} = the number of "point-like" spectators to the emission and n_H = the number of "hadronic" spectators. Hadronic spectators are those quarks which are connected to other quarks in the emitted bound state (or to quarks in an initial bound state, when present) by an explicit gluon exchange; in other words, hadronic spectators are spectator quarks which are internally connected to either an initial or a final bound state. In contrast, point-like spectators are those obtained by a bremstrahlung from an initial, incoming quark line. Thus in Fig. 18(a), $n_H = 1$, $n_{PL} = 0$; in Fig. 18(b), $n_H = 0$, $n_{PL} = 3$. A less elementary diagram for obtaining $u \to \pi^-$ is shown in Fig. 18(c). It employs a higher Fock state of the π^- and has $n_H = 3$, $n_{PL} = 0$ yielding $(1 - x)^5$ in disagreement with experiment. This is the prediction of the earliest version of the spectator counting rules[31] which did not take into account possible point-like emissions. The relative normalization of the contributions is not presently known but experiment clearly prefers the point-like emission diagram. A final mechanism for $u \to \pi^-$ is via resonance decay $u \to \rho^0 \to \pi^-$, Fig. 18(d), which also yields $(1 - x)^2$, the same result as the point-like graph, Fig. 18(b). It is conceivable that the point-like

contribution is small and that all π^- production comes from this source. Experimental attempts to resolve this question would be very useful.

Turning to diquark fragmentation, the leading diagram for $(uu) \to \pi^+$ is the point-like mechanism shown in Fig. 18(e), yielding $(n_{PL} = 2, n_H = 0)$

$$\left.\frac{dN}{dx}\right|_{PL}^{uu \to \pi^+} \sim (1 - x) \quad . \tag{3.9}$$

A possibly important background diagram is given in Fig. 18(f), where a fast u quark decays to the observed π^+; it yields $(n_H = 2, n_{PL} = 0)$

$$\left.\frac{dN}{dx}\right|_{H}^{uu \to \pi^+} \sim (1 - x)^3 \quad . \tag{3.10}$$

Resonance ρ^o production via the point-like mechanism followed by decay yields

$$\left.\frac{dN}{dx}\right|_{\rho^o}^{uu \to \pi^+} \sim (1 - x)^2 \quad . \tag{3.11}$$

The data appears to show some combination of these, but a precise determination of their relative weight is difficult. It should be noted that the possible presence of $q\bar{q}$ sea pairs and gluons in the fragmenting deep inelastic diquark system does not modify the leading power predictions above, provided these extra particles participate in forming the π^+. On the other hand, if some are lost in radiation the uu-system which emits the π^+ carries less momentum and finds it more difficult to make the π^+. This would result in contributions based on each of the above basic mechanisms with higher powers than for the leading diagrams. These contributions might be significant. As an example, suppose a complicated uu-system first emits a bare uu diquark which in turn fragments in point-like fashion to the observed π^+, Fig. 19. One must then compute dN/dx as

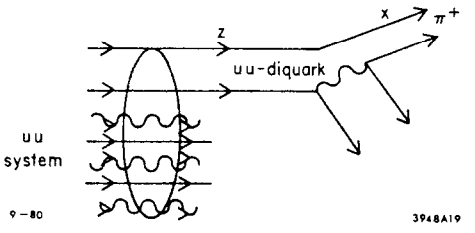

Fig. 19. Fragmentation of a complicated uu-system to a bare uu diquark which in turn fragments to the observed π^+.

$$\frac{dN}{dx}^{(uu\text{-system}) \to \pi^+} = \int_x^1 \frac{dz}{z} G_{uu/uu\text{-system}}(z)\, G_{\pi^+/uu}(x/z) \qquad (3.12)$$

The form of $G_{\pi^+/uu}(x/z)$ is taken from the point-like prediction of Eq. (3.9) as

$$G_{\pi^+/uu}(x/z) \sim (1 - x/z) \quad . \qquad (3.13)$$

The form of $G_{uu/uu\text{-system}}(z)$ depends upon the complexity of the uu-system; let us presume that it is z independent. Then Eq. (3.13) combined with Eq. (3.12) yields the observed spectrum, Eq. (3.2). Eventually as $x \to 1$ this mechanism must become less important than that in which all the gluons and $q\bar{q}$ sea pairs participate in forming the pion, and we obtain the point-like answer of Eq. (3.9).

For $(uu) \to \pi^-$ the point-like diagram is given in Fig. 18(g) ($n_H = 0$, $n_{PL} = 4$) yielding[34]

$$\left.\frac{dN}{dx}\right|_{PL}^{uu \to \pi^-} \sim (1 - x)^3 \qquad (3.14)$$

The diagram which yields the old spectator counting results[31] is shown in Fig. 18(h) ($n_H = 4$, $n_{PL} = 0$)

$$\left.\frac{dN}{dx}\right|_{H}^{uu \to \pi^-} \sim (1 - x)^7 \quad . \qquad (3.15)$$

The possibility $uu \to \rho^0 \to \pi^-$ of Fig. 18(i) yields

$$\left.\frac{dN}{dx}\right|_{\rho^0}^{uu \to \pi^-} \sim (1 - x)^2 \quad . \qquad (3.16)$$

The data of Fig. 16. is most consistent with the point-like diagram result. In much of what follows we will adopt the point-like diagram approach for all fragmentations. One should, however, keep in mind some of the above subtleties.

Theoreticians should note that all diagrams shown in Fig. 18 are actually the "Born" contributions. The theoretical analysis is done along the lines applied by Brodsky and Lepage[35] to the pion form factor. The bound state ladder graph corrections to the "Born" expressions given above are inconsequential for semi-quantitative phenomenology. A bit more discussion will be given momentarily.

ii) The Valon-Recombination Approach

It is useful at this early stage to compare our $x \to 1$ QCD approach to the QCD based Valon apprach to fragmentation. The idea there is that the physics which dominates as $x \to 1$, while

appropriate in the limit, does not correspond to the dominant physics at moderate x. Consider the example of u quark fragmentation to a π^+. The recombination approach is based on the diagram shown in Fig. 20. Here the initial quark (created by a momentum transfer Q^2 probe) has its linear momentum degraded from

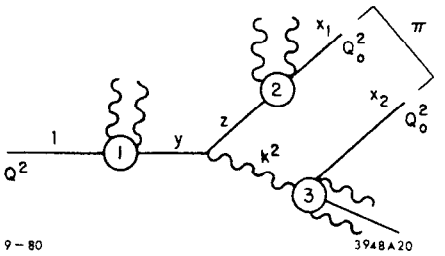

Fig. 20. The basic diagram for quark fragmentation to a pion. Intermediate radiation occurs at locations 1, 2 and 3 which will be used to label distribution functions in the relevant equation, (3.17).

1 to y by gluon radiation. It then emits a hard gluon of momentum transfer k^2 and linear momentum y-z leaving behind a quark with linear momentum z. The (y-z) gluon and z quark now radiate; the z quark yields a final quark of linear momentum x_1 at momentum transfer scale Q_0^2 while the (y-z) gluon yields an antiquark of linear momentum x_2 at momentum transfer scale Q_0^2. The formula reads ($x_1 + x_2$ is the π momentum)

$$\frac{dN}{d(x_1+x_2)} \sim \int_{Q_0^2}^{Q^2} dk^2 \int_{x_1+x_2}^{1} dy \int_{x_1}^{1-x_2} \frac{dz}{y} \left[G_{q/q}(y,Q^2,k^2) \right]_1$$
$$\times P_{q/q}(z/y)\, \frac{\alpha(k^2)}{k^2} \left[\frac{x_1}{z} G_{q/q}\left(\frac{x_1}{z}, k^2, Q_0^2 \right) \right]_2$$
$$\times \left[G_{\bar{q}/g}\left(\frac{x_2}{y-z}, k^2, Q_0^2 \right) \right]_3 \qquad (3.17)$$

The subscripts refer to the various radiation blobs in Fig. 20. The radiation G's are the solutions to the standard evolution equations describing the quark content of a primary quark or gluon. The k^2 variable of the hard gluon relative to the initial Q^2 or final Q_0^2 momentum transfer scales sets the amount of evolution allowed in each of the G's. The $P_{q/q}(z/y)\alpha(k^2)/k^2$ factor describes the emission of the hard "pair creating" gluon. The momentum of the final pion is $x_1 + x_2$. As $(x_1 + x_2) \to 1$ all three G's are forced to their end points ($y \to 1$, $x_1 \to z$, $x_2 \to y-z$) and their are two integral convolutions in (3.17) each of which yields an additional single power suppression in the limit.

The $P_{q/q}$ distribution is not forced to its end point. Consider for example the particular k^2 value of $k^2 = Q_0^2$. Only $G_{q/q}(y)$ has any evolution. The other G's are given by their lowest order expressions. We have, roughly,

$$G_{q/q}(y) \approx (1-x_1-x_2)^{\xi(Q^2,Q_0^2)-1}$$

$$G_{q/q}(x_1/z) \approx (1-x_1-x_2)^{-1} \tag{3.18}$$

$$G_{\bar{q}/g}(x_2/(y-z)) \approx (1-x_1-x_2)^{0}$$

where (Λ = the standard QCD parameter)

$$\xi(Q^2,Q_0^2) = \frac{16}{33-2n_f} \ln \frac{\ln[Q^2/\Lambda^2]}{\ln[Q_0^2/\Lambda^2]}$$

is the standard evolution parameter. Combining the above with the two extra powers of $(1-x_1-x_2)$ coming from the two convolutions yields (with $x = x_1 + x_2$)

$$\frac{dN^{q\to\pi}}{dx} \underset{x\to 1}{\sim} (1-x)^{\xi(Q^2,Q_0^2)+1} \tag{3.19}$$

For $Q = 5$, $\Lambda = .5$ GeV and $Q_0 = .5$ GeV, ξ is ≈ 1 and

$$\frac{dN^{q\to\pi}}{dx} \sim (1-x)^2 \quad . \tag{3.20}$$

Thus all the convolutions and radiations combine to give reasonable agreement with experiment.

It should be apparent that the diagram of Fig. 20 is not much different from the QCD "Born" graph of Fig. 18(a), which yields the point-like counting rules. In fact if we merely neglect the evolution factor, ξ, both approaches would yield (in the spinless approximation in which we are working) the same power law behavior

$$\frac{dN^{q\to\pi}}{dx} \underset{x\to 1}{\sim} (1-x) \quad . \tag{3.21}$$

This phenomenological similarity does not mean that the physics is the same. To understand the relationship between the two approaches one first notes that if the x_2 quark in the pion of Fig. 20 is more or less on-shell (as it must be in a bound state)

then as $x_2 \to (y-z)$, as required in the $x_1 + x_2 \to 1$ limit, the gluon k^2 is actually not a free parameter but is determined by $(1-x_1-x_2)$:

$$k^2 \approx \frac{k_\perp^2}{1 - \frac{x_2}{y-z}} \propto \frac{k_\perp^2}{1-x_1-x_2} \tag{3.22}$$

where $k_\perp$ is a typical constituent transverse momentum. As $x_1 + x_2 \to 1$, k^2 eventually becomes as large as Q^2 and radiation at site 1 is suppressed. The radiation at sites 2 and 3 is still allowed and one would obtain

$$\left.\frac{dN}{dx}\right|_{\text{Valon}}^{q \to \pi} \sim (1-x)^{1 + 2\xi\left(k^2, Q_0^2\right)} \tag{3.23}$$

from the diagram of Fig. 20. That is, the damping as $x \to 0$ is stronger than that for the diagrams without any extra gluon radiation, Fig. 21, in which only internal bound state ladder graph corrections are allowed. These graphs yield the point-like result Eq. (3.21). Thus as $x \to 1$ the "exclusive" graphs of the type shown in Fig. 21 dominate[37] over graphs of the "inclusive" type considered in the Valon approach, Fig. 20, where extra gluon radiation (leading to extra ξ's in the power law) from the basic "Born" graph is allowed. Which type of graph dominates at moderate x is a matter of normalization; only as $x \to 1$ can it be definitively proven that "exclusive" graphs dominate. Rough estimates suggest that at $x = .5$ the two types of graph contribute approximately equal amounts to the $q \to \pi$ distribution. Other comparisons between the two approaches will appear later. The above $q \to \pi$ example is simplest as no possibly unknown "primordial" distributions enter into the comparison. This will not be the case in considering hadron jet fragmentation.

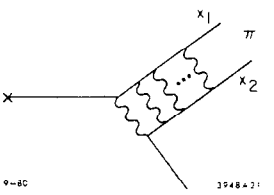

Fig. 21. The general "exclusive" graph for $q \to \pi$ in which no excess gluon radiation appears.

B) Hadronic Collision Fragmentation

i) The Dual Model Approach[3,4,5]

It is now possible to discuss systematically the fragmentation distributions for purely hadronic collisions. It is convenient to begin with the possibilities which arise in the dual

Pomeron model approaches. In the extreme first considered by Anderson et al,[3] the diquark in the proton carried all the momentum of the proton and the quark had none. The fragmentation spectrum of a meson from a proton would then be equal to that from a diquark (or more generally a diquark system including gluons, etc.)

$$\frac{dN^{pp \to \pi}}{dx} \sim \frac{dN^{2q \to \pi}}{dx} . \tag{3.24}$$

We have seen that deep inelastic scattering measures the fragmentation spectrum of a diquark-system with the result that

$$\frac{dN^{(2q\text{-system}) \to \pi}}{dx} \sim (1-x)^2 \tag{3.25}$$

for a favored fragmentation; the power could be lower for a pure diquark. The proton data for $pp \to \pi^+$ does not agree with this. Instead we find experimentally

$$\frac{dN^{pp \to \pi^+}}{dx} \sim (1-x)^3 . \tag{3.26}$$

Typical data is shown in Fig. 22.[38] A small mixture of a higher power is required to fit the data with complete precision, but certainly the lower power of Eq. (3.24) is ruled out.

Of course, in a more realistic version of the dual model approach, it is recognized[3,4,5] that some penalty must be payed if the diquark is to carry all the momentum. In fact there is a distribution of the diquark momentum related to the slowed-quark distribution given earlier in Eq. (2.17) or (2.19). One must convolute the distribution of the diquark inside the proton with the fragmentation distribution for a pion inside a diquark, see Fig. 23(a).

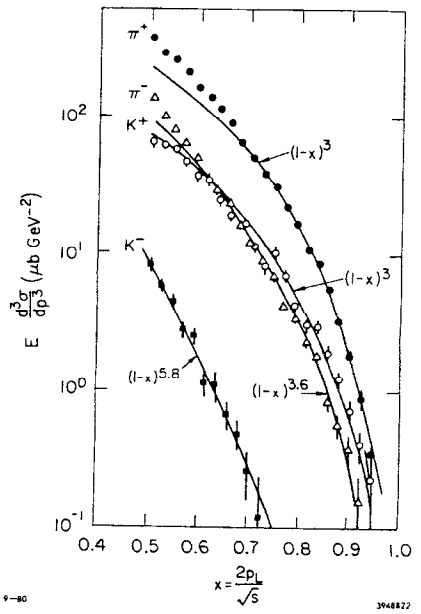

Fig. 22. Comparison of invariant cross section for $pp \to \pi^+$, π^-, K^+, K^-, from Ref. 38. Single power curves are drawn.

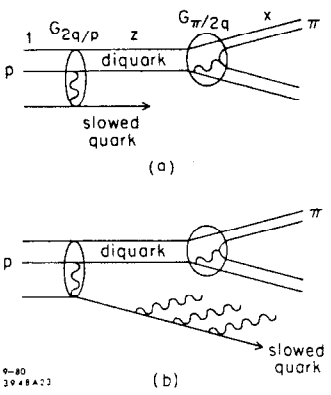

Fig. 23. Diagrams for the two stage picture of pion emission from a scattering proton. In a) all the momentum not carried by the slowed quark is carried by the diquark which in turn emits the pion. In b) the diquark does not carry all the left over momentum; some is lost in gluon radiation.

The resulting pion distribution is given by

$$\frac{dN^{p\to\pi}}{dx} = \int_x^1 \frac{dz}{z} G_{2q/p}(z)\, G_{\pi/2q}(x/z) \ . \quad (3.27)$$

By symmetry we have

$$G_{2q/p}(z) = \hat{G}_{q/p}(1-z) \quad . \quad (3.28)$$

where $\hat{G}_{q/p}$ is the distribution of the quark left behind by the 2q emission from the proton. If we assume that in a hadron collision there is no emission from the quark line after the diquark system, which radiates the pion, has been isolated then $\hat{G}_{q/p}$ should be identified with $G_{q/p}$ of Eq. (2.17) or (2.19) describing the distribution of momentum for the slowed quark. This, however, is not generally true. The quark can in general radiate additional gluons, subsequent to the proton's emitting the diquark system, and be further slowed down. This possibility is illustrated in Fig. 23(b). Thus $\hat{G}_{q/p}$ is the quark distribution prior to the additional gluon radiation. Based on QCD, $\hat{G}_{q/p}$ should be closely related to the valence Fock state quark distribution, Eq. (2.17), and

$$G_{2q/p}(z) = \hat{G}_{q/p}(1-z) = G^V_{q/p}(1-z) \propto z^3(1-z) \ ; \quad (3.29)$$

whereas $G_{q/p}$ after the radiation could have the Regge or other $x \to 0$ singular behaviour of Eq. (2.19).

Thus from a diagrammatic QCD point of view one should employ $G_{\pi/2q}(x/z)$ as given by the point-like distribution Eq. (3.9) and use $G_{2q/p}$ as determined in QCD for the valence quark distribution, Eq. (3.29). This yields a pion distribution, from Eq. (3.27), of

$$\frac{dN^{p\to\pi}}{dx} = \int_x^1 \frac{dz}{z} \left[(1-z)z^3\right]\left[\left(1-\frac{x}{z}\right)\right] \underset{x\to 1}{\sim} (1-x)^3 \ . \quad (3.30)$$

The convolution supplies the extra power. This result agrees with with the data. It could be argued that the experimental result for $G_{\pi/2q}$, Eq. (3.2), as measured in deep inelastic scattering, should be employed yielding a phenomenologically less successful form

$$\frac{dN^{p \to \pi}}{dx} \sim (1-x)^4 \tag{3.31}$$

when combined with the valence form of $\hat{G}_{q/p}$. This is not obviously correct, however, as the 2q-system in deep inelastic scattering is, on the average, much more complicated than the simple diquark appearing here. The effect of this was discussed with regard to Eq. (3.12).

In the literature the dual models[5] have taken the Regge form for $\hat{G}_{q/p}$ and the spectator counting rule form of $G_{\pi/2q}$, Eq. (3.10). This yields

$$\frac{dN^{p \to \pi}}{dx} = \int_x^1 \frac{dz}{z} \frac{z^3}{\sqrt{1-z}} \left(1 - \frac{x}{z}\right)^3 \overset{x \to 1}{\sim} (1-x)^{3.5} \tag{3.32}$$

which is also not in bad agreement with experiment. Using a Regge form for $\hat{G}_{q/p}$ might actually be appropriate if the radiated gluons of Fig. 23(b) were to be considered as part of the diquark system and if one used an appropriate form for $G_{\pi/2q\text{-system}}$ (in place of $G_{\pi/2q}$ in Eq. (3.27)) which accounted for the more complicated nature of the diquark system radiating the pion. Further theoretical analysis of this possibility is needed. The $(1-z)^{-\frac{1}{2}}$ behavior of $G_{2q\text{-system}/p}$ arises via a superposition of proton Fock states with different numbers of radiated gluons; as $z \to 1$ the 2q-system which, in this alternative, is to include these gluons is growing in complexity and $G_{\pi/2q\text{-system}}$ is changing. The convolution analogous to Eq. (3.27) is thus very subtle. As $x \to 1$, QCD predicts that the point-like contribution based on Fig. 23(a) and discussed earlier should dominate but at moderate x contributions involving complicated diquark systems could be significant.

ii) The Gluon Exchange with Point-Like QCD Emission Approach[34]

The gluon exchange QCD model basically operates in the fragmentation region much like the dual Pomeron model. In proton

fragmentation to a pion one has a proton-like 3-quark state traveling in the forward direction which then emits a pion using a point-like QCD bremstrahlung process. The leading diagram is that given in Fig. 24. There are $n_H = 1$ hadronic spectators and $n_{PL} = 2$ point-like spectators with the result

$$\frac{dN^{p\to\pi}}{dx} \sim (1-x)^3 \quad . \qquad (3.33)$$

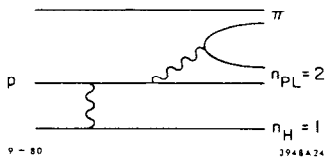

Fig. 24. Leading QCD diagram for π emission from a proton state.

As we have seen in discussing Fig. 23(a) this same result can be equivalently viewed as a two stage process of: 1) 2q emission from the proton according to the QCD predicted valence distribution of Eq. (3.29), and 2) pion emission from the 2q according to the point-like QCD bremstrahlung prediction of Eq. (3.9). The n_H, n_{PL} counting rules simply summarize the results of such a calculation. Thus, in principle, the two approaches are completely equivalent as $x \to 1$. At moderate x the Regge behavior subtleties, as discussed previously, may lead to some differences in practice.

iii) The Valon Model[39]

The valon model is also very closely related to the previous two approaches. The proton, as in the dual model and gluon exchange theories, is viewed as being essentially undistrubed by the hadron collision mechanism; fragmentation of the pion is viewed as the recombination of a quark and antiquark which are contained within the proton state. The dominant basic diagram is given in Fig. 25(a), a contribution to which is drawn in Fig. 25(b). The similarity to the point-like diagram of

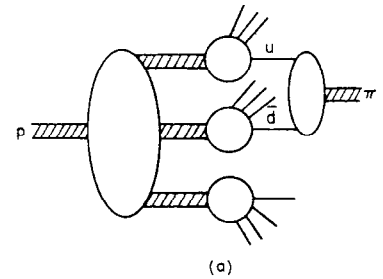

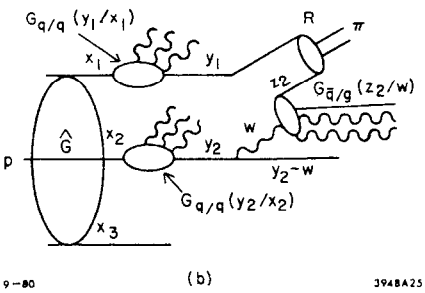

Fig. 25. The Valon picture of pion fragmentation from a proton. The general diagram is drawn in a) and a specific contribution analogous to Fig. 24 is shown in b).

Fig. 24 should be obvious. One calculates the pion distribution predicted by Fig. 25(b) as a convolution of:

a) the distribution of the three valons of momentum x_1, x_2 and x_3 in the basic proton, $\hat{G}(x_1,x_2,x_3)$;

b) the probability for valon 1 to have momentum y_1 after some QCD determined radiation, $G_{q/q}(y_1/x_1)$;

c) the probability for valon 2 to have momentum y_2 after some QCD determined radiation $G_{q/q}(y_2/x_2)$;

d) the probability for hard pair creating gluon emission of momentum w, $P_{g/q}(w/y_2)$;

e) the probability $G_{\bar{q}/g}(z_2/w)$ for the hard gluon carrying w to radiate a $\bar{q}$ of momentum z_2;

f) the probability $R_x(y_1,z_2)$ for the y_1-quark and z_2-antiquark to recombine to form a pion with momentum x.

Each of the G's is taken to have a QCD evolved form and $P_{g/q}$ is taken to be given by the QCD Born expression. The only unknowns are the original valon distribution $\hat{G}$ and the recombination function R which are adjusted to agree with deep inelastic and e^+e^- annihilation data. The $x \to 1$ behavior is not sensitive to R except as to normalization. The form of G is important. QCD predicts[27] that as x_3 is forced to 0 (required when $x \to 1$)

$$\hat{G}(x_1,x_2,x_3) \propto x_1x_2x_3\ \delta(1-x_1-x_2-x_3) \tag{3.34}$$

which is equivalent to the valence diquark distribution

$$\begin{aligned} G_{2q/p}(z) &= \int dx_1\,dx_2\,dx_3\ \delta(z-x_1-x_2)\ \hat{G}(x_1,x_2,x_3) \\ &= \int_0^z dx_1\ x_1(z-x_1)(1-z) \\ &\propto z^3(1-z) \end{aligned} \tag{3.35}$$

quoted in Eq. (3.29). In fact if we neglected the evolution in each of the G's of (b), (c) and (e), above, and used this form of $\hat{G}$ one would obtain exactly the point-like prediction for $p \to \pi$, Eq. (3.33)/Eq. (3.30). This should be very reminiscent of the Valon vs. QCD comparison for $q \to \pi$. If we turn on evolution in the G's, as is done in the Valon approach, it is necessary to weaken the damping contained in $\hat{G}(x_1,x_2,x_3)$ in order to obtain agreement with experimental deep inelastic $x \to 1$ behavior and with

the $p \to \pi$ experimental distribution. The form

$$\hat{G}(x_1,x_2,x_3) \approx (x_1x_2)^{.08}\, x_3^{.12}\, \delta(1-x_1-x_2-x_3)\ , \qquad (3.36)$$

where x_1 and x_2 label the u-type valons and x_3 the d-type valon, is used. This form has weaker damping than predicted in QCD, which compensates phenomenologically for the extra evolution in the G's, yielding an excellent description of deep inelastic and $pp \to \pi$ data. As in the $q \to \pi$ discussion, in the strict limit of $x \to 1$, the "inclusive" radiation graphs of the type drawn in Fig. 25 and used in the Valon approach are suppressed[37] relative to "exclusive" graphs in which no extra radiation occurs. The weak damping form of $\hat{G}$ given in (3.36) would then yield

$$\frac{dN^{p \to \pi}}{dx} \underset{\sim}{x \to 1} (1-x)^2 \qquad (3.37)$$

whereas the QCD form of $\hat{G}$ yields a prediction which connects smoothly to the observed data in the range $.5 < x < .9$.

The slight differences between the three theoretical approaches — dual model, QCD "exclusive" graphs, and Valon model ("inclusive" QCD graphs) — should not obscure the fundamental similarity of all three. In all three approaches a colliding hadron state is essentially undisturbed by the collision and then fragments according to QCD based graphs. As time progresses I expect more and more consensus concerning the exact numerical details of how to compute the various contributions represented by the above three models.

iv) Summary of Gluon Exchange and Point-Like QCD Emission Results for all Fragmentations.[34]

In the above model comparison I have, of course, focused on the single case of $p \to \pi$ fragmentation. Each of the above models must address other fragmentations such as $p \to K^-$, $K^- \to p$, $p \to \bar{\Lambda}$ and $\pi^- \to \pi^+$, to name a few exotic cases. The phenomenology for the dual model and Valon approaches has been presented in other talks at this conference. Let me spend a few pages summarizing the status of the QCD "exclusive" diagram approach. As in the cases discussed so far one searches for the "exclusive" QCD diagram which predicts the minimum damping as the fragment momentum fraction, x, approaches 1. This power law, which can be

shown to dominate as $x \to 1$, is then compared to the data at large x, $x > .5$.

To illustrate let us consider the three cases mentioned above. The leading diagrams are shown in Fig. 26, along with

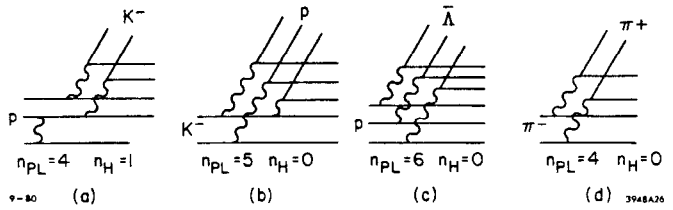

Fig. 26. Leading diagrams for the fragmentations: a) $p \to K^-$; b) $K^- \to p$; c) $p \to \bar{\Lambda}$ and d) $\pi^- \to \pi^+$, respectively.

the spectator numbers. Applying Eq. (3.8) we obtain

$$\left.\frac{dN}{dx}\right|_{\substack{\text{QCD}\\ \text{leading}\\ \text{diagram}}} \sim \begin{cases} (1-x)^5 & p \to K^- \\ (1-x)^4 & K^- \to p \\ (1-x)^5 & p \to \bar{\Lambda} \\ (1-x)^3 & \pi^- \to \pi^+ \end{cases} \tag{3.38}$$

Averaging the various experimental results[40] we have

$$\left.\frac{dN}{dx}\right|_{\text{Experimental}} \sim \begin{cases} (1-x)^{5.5} & p \to K^- \\ (1-x)^4 & K^- \to p \\ (1-x)^8 & p \to \bar{\Lambda} \\ (1-x)^3 & \pi^- \to \pi^+ \end{cases} \tag{3.39}$$

Except for $p \to \bar{\Lambda}$ the predictions of the leading QCD diagrams are remarkably similar to experiment. Particularly noteworthy is the predicted and observed difference between $p \to K^-$ and $K^- \to p$ which would not be anticipated in the earlier multiperipheral and triple Regge theories where the controlling (exotic) trajectory should have been the same in the two cases. The $p \to \bar{\Lambda}$ failure should not, as we have learned, be taken as a failure of QCD but rather as a failure of the leading QCD diagram, which dominates as $x \to 1$, to dominate at moderate x where the measurements are performed. A failure of QCD requires observation of a weaker power law than that predicted by the leading diagram.

A global summary of data available prior to this conference[40] together with the leading QCD diagram predictions is given in Fig. 27. In Fig. 28(a) I show sample data presented at

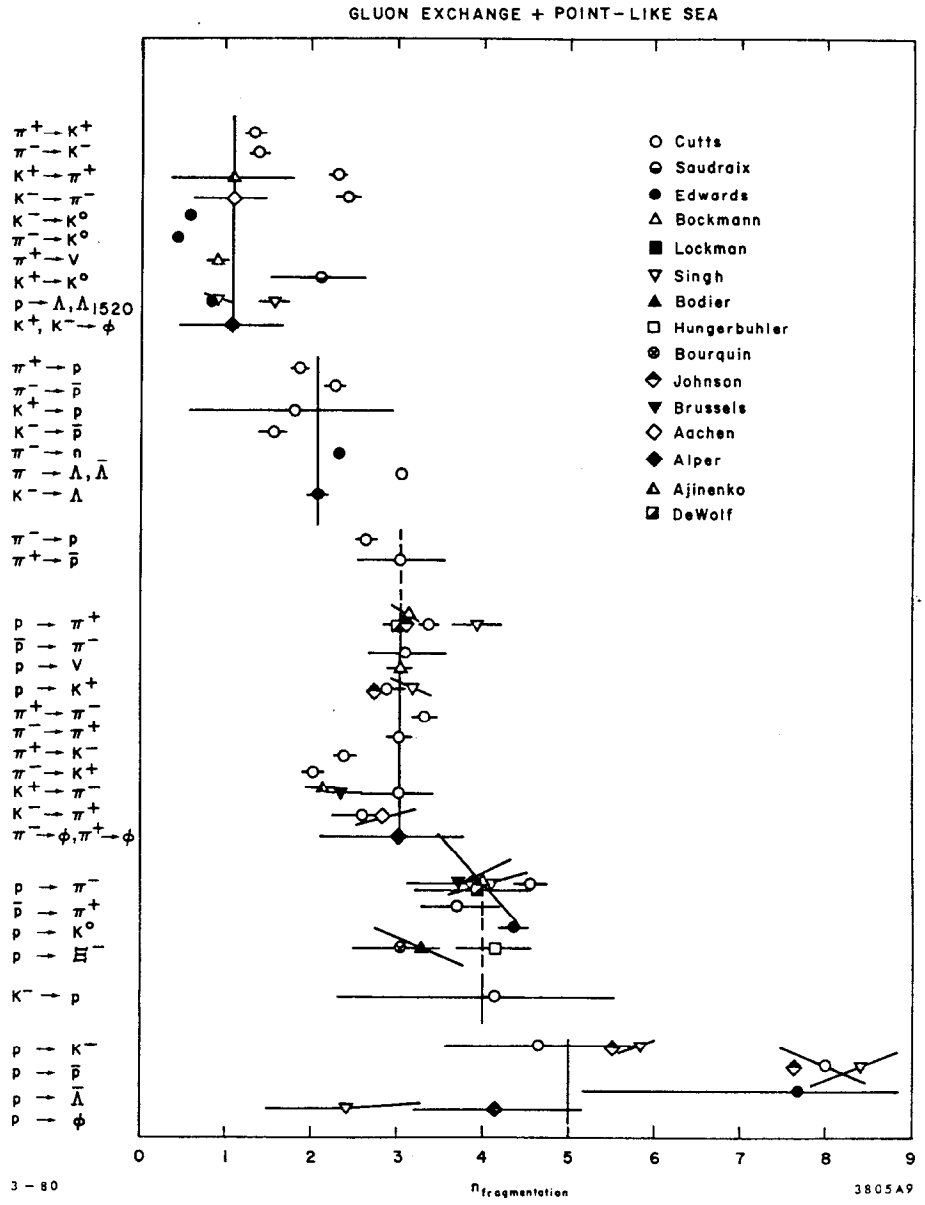

Fig. 27. A summary of experimental results[40] and theoretical predictions in the gluon exchange model for all available single particle fragmentations. Here solid lines indicate predictions for gluon exchange and point-like pair creation. Broken lines indicate that one unit has been added to the naive point-like prediction because a proton's d-quark is used in the fast fragmentation.

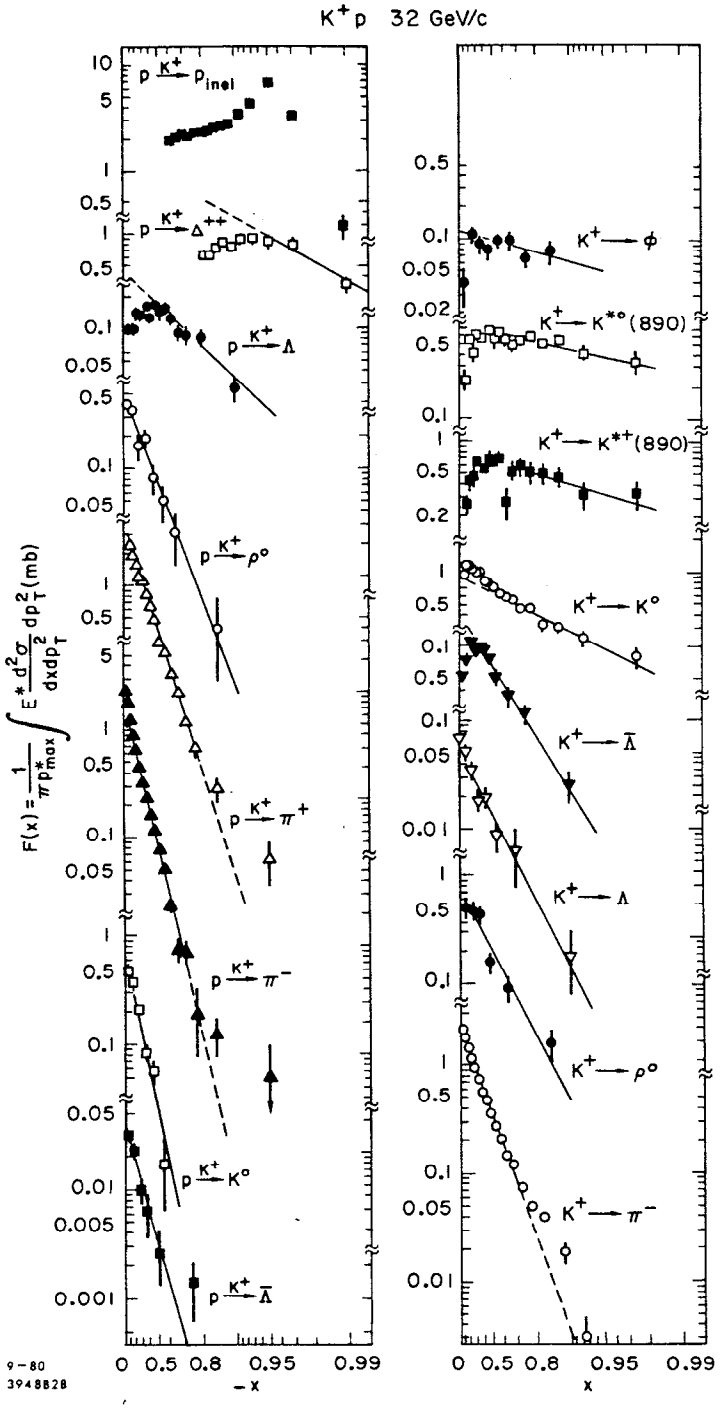

Fig. 28(a).

We show forward and backward fragmentation distributions obtained in K^+p interactions. The solid lines indicate the range over which fits were actually performed to obtain n in $(1-x)^n$. K^-p interactions were also measured.

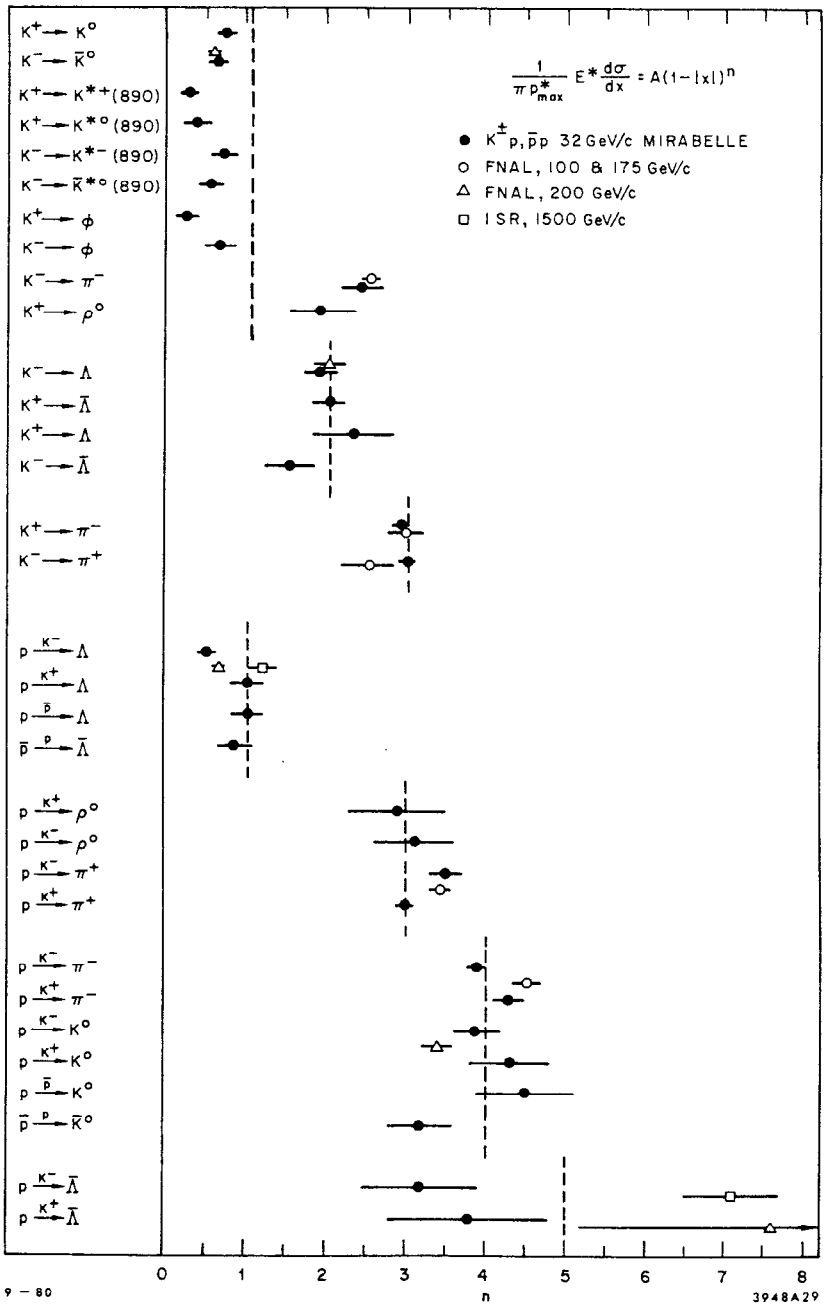

Fig. 28(b). We show the comparison between the leading QCD diagram $x \to 1$ power law predictions and the above experimental determinations of n. The dotted lines indicate the theoretical predictions.

this conference[41] together with some power law fits and compare the fitted power law to the leading QCD predictions in Fig. 28(b). The over all agreement seems quite good. The slightly low powers for K fragmentation to a meson containing a strange quark can probably be attributed to mass effects related to the presence of one heavy and one light quark in the K meson. This leads to a distorted x distribution at moderate x which can explain the observations.

v) Factorization and the Elimination of Various Alternative Models.

So far we have focused only on three models in which backward and forward fragmentation regions factorize from one another. This is, of course, required by the experiment of Bobink et al.[6] They observe no correlation between two pion fragments, π_1 and π_2, one observed with $x_F^1 > 0$ and the other with $x_F^2 < 0$. The experiment shows that in pp collisions

$$R \equiv \frac{\frac{1}{\sigma} E_1 E_2 \frac{d\sigma}{d^3p_1 d^3p_2}}{\frac{1}{\sigma} E_1 \frac{d\sigma}{d^3p_1} \frac{1}{\sigma} E_2 \frac{d\sigma}{d^3p_2}} = 1 \qquad (3.40)$$

to a good approximation. Let us compare this prediction of a gluon exchange model to expectations for a model of the Fig. 1(c) type — valence quark absorption of a sea quark. If we produce π_1 and π_2 fragments the leading diagram is illustrated in Fig. 29 for a pp collision. Assuming that q' is slow and should not be counted among the spectators, the n_H and n_{PL} values are as shown. We obtain after symmetrizing ($x_1 \equiv |x_F^1|$, $x_2 \equiv |x_F^2|$)

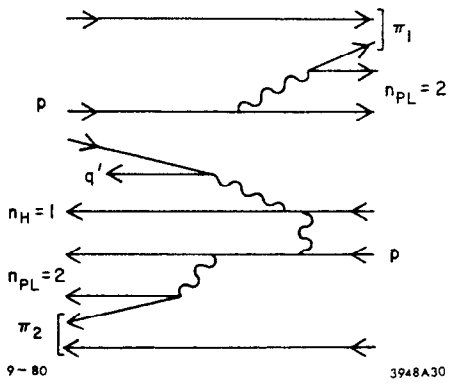

Fig. 29. The leading diagram for pp collisions producing a forward and backward pion simultaneously when the collision mechanism is of the Fig. 1(c) type.

$$R = \frac{(1-x_1)(1-x_2)^3 + (1-x_2)(1-x_1)^3}{(1-x_1)(1-x_2)}$$

$$= (1-x_2)^2 (1-x_1)^2 \qquad (3.41)$$

which violates factorization badly. Note that for the single variable cross sections we must use the leading result, given by the top half of Fig. 29, which yields ($n_{PL} = 2$)

$$\frac{dN^{p \to \pi}}{dx} \sim (1-x) \qquad (3.42)$$

which is also in disagreement with experiment. If the q' spectator were to be considered part of the backward jet, i.e., if it is speeded up so as to move with its neighbors before the fragmentation occurs, n_H would be increased by one unit in the backward direction and the violation of factorization would be even more severe. Thus the experimental observation of factorization appears to rule out this type of hadron interaction diagram which, as discussed in Sec. II, yields the most natural explanation of the leading proton and πp multiplicity relationships discussed around Eqs. (2.11) and (2.13).

The other interaction mechanism capable of explaining the multiplicity regularities, referred to above, in a natural way is illustrated in Fig. 1(b). As discussed in Sec. II, in order to explain the regularities, the q' and $\bar{q}'$ quarks must both be fast so that the forward and backward jets are radiating as color triplets, see Eq. (2.7). In this case the fragmentation picture for pp collisions is shown in Fig. 30. From the leading top

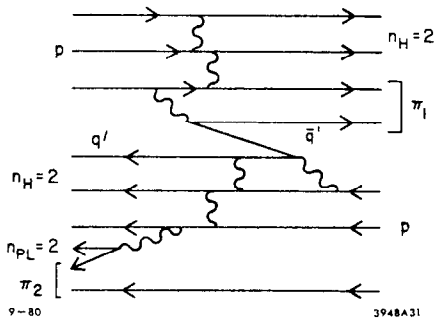

Fig. 30. Fragmentation to a forward and backward pion when the interaction mechanism is the exchange of a sea quark as in Fig. 1(b).

half of the diagram we obtain

$$\frac{1}{\sigma} E \frac{d\sigma}{d^3p}^{pp \to \pi} \equiv \frac{dN^{p \to \pi}}{dx} \sim (1-x)^3 \tag{3.43}$$

in agreement with experiment; but for R one obtains (after symmetrizing)

$$R = \frac{(1-x_1)^3 (1-x_2)^5 + (1-x_1)^5 (1-x_2)^3}{(1-x_1)^3 (1-x_2)^3} \tag{3.44}$$

which, again, strongly violates factorization. Only if q' were slow and $\bar{q}'$ fast would we obtain factorization; but this would destroy the desireable multiplicity pattern discussed in Sec. II.

IV. Summary

Thus, in final summary, the only QCD interaction mechanism capable of producing reasonable results for the multiplicity, correct power laws for fragmentation functions, and forward-backward fragmentation factorization is the gluon exchange mechanism illustrated in Fig. 1(a). The other phenomenologically successful approaches to both the multiplicity and the fragmentation region have many features which are quite similar to the combination of this elementary QCD interaction mechanism with point-like emission diagrams for fragmentation. Theorists need to devote additional effort to justifying these simple pictures. The most nagging problems are: A) the role played by higher Fock states of the colliding hadron — these contain gluons which can scatter in a way which complicates the multiplicity pictures; and B) the role played by multiple exchanges in the elementary QCD exchange approach.

Acknowledgments: I would like to thank the organizers of the Brügge Symposium for their kind hospitality. I would also like to thank S. J. Brodsky, S. Pokorski, N. Schmitz, G. Wolf, A. Capella and N. Sukhatme for helpful conversations.

References

1. F. E. Low, Phys. Rev. D12, 163 (1975); S. Nussinov, Phys. Rev. Lett. 34, 1286 (1975); J. F. Gunion and D. E. Soper, Phys. Rev. D15, 2617 (1977).
2. S. J. Brodsky and J. F. Gunion, Phys. Rev. D17, 848 (1978); Phys. Rev. Lett. 37, 402 (1976); Phys. Rev. D19, 1005 (1979).
3. B. Andersson, G. Gustafson and C. Peterson, Phys. Lett. 71B, 337 (1977) and Phys. Lett. 69B, 221 (1977); B. Andersson, G. Gustafson, I. Holgersson, O. Mansson LU-TP-80-5 (1980).
4. G. Cohen-Tannoudji, A. El Hassouni, J. Kalinowski, O. Napoly and R. Peschanski, Phys. Rev. D21, 2699 (1980) and earlier references therein; A. El Hassouni and R. Peschanski, 14th Rencontre de Moriond, Les Arcs, France, 1979, p. 571; R. Peschanski, this conference; H. Minakata, Phys. Rev. D20, 1656 (1979).
5. A. Capella, U. Sukhatme and J. Tran Thanh Van, Zeitschrift für Physik C, 329 (1980); A. Capella, presented at this Conference.
6. G. J. Bobink et al., Phys. Rev. Lett. 44, 118 (1980).
7. See the talk by Chliapnikov at this Conference. See also S. Nandi, V. R. Henberg, H. Schneider, Phys. Rev. D17, 1336 (1978).
8. See J. F. Gunion and D. E. Soper in Ref. 1; and J. F. Gunion and S. J. Brodsky, Phys. Rev. D19, 1005 (1979).
9. R. C. Brower, W. L. Spence and J. Weis, Phys. Rev. D19, 3024 (1979); R. C. Brower et al., Nucl. Phys. B128, 131 and 175 (1977); R. C. Brower, J. Ellis, M. Schmidt and J. Weis, Phys. Lett. 65B, 249 (1976).
10. S. J. Brodsky and J. F. Gunion, Phys. Rev. Lett 37, 402 (1976), and Proceedings of Tutzing Conference — 7th Int. Colloquium on Multiparticle Reactions, Munich, 1976; see also J. Dash, Phys. Rev. D19, 3472 (1979).
11. G. C. Fox and S. Wolfram, Nucl. Phys. B168, 285 (1980) and S. Wolfram, 15th Rencontre de Moriond, Les Arcs, France, 1980; K. Konishi, A. Ukawa, G. Veneziano, Phys. Lett. 78B, 243 (1978); K. Konishi, 11th Int. Symp. on Multiparticle Dynamics, Brügge, Belgium, 1980; P. Cvitanovic, P. Hoyer, K. Konishi, Phys. Lett. 85B, 413 (1979); B. Andersson, G. Gustafson, T. Sjostrand, LU-TP-80-1 (1980); B. Andersson, G. Gustafson, C. Peterson, Phys. Scr. 19, 184 (1979).

12. W. Furmanski, S. Pokorski, Nucl. Phys. B155, 253 (1979); A. Bassetto, M. Ciafaloni, G. Marchesini, Phys. Lett. 83B, 207 (1978).
13. C. B. Chiu, 14th Rencontre de Moriond, Les Arcs, France, 1979, Vol. 2, p. 587; A. Casher, H. Neuberger, S. Nussinov, Phys. Rev. D20, 179 (1979).
14. J. F. Gunion, in preparation. See also, J. F. Gunion, Proceedings of the 13th Rencontre de Moriond, Les Arcs, France, 1978, Vol 1, p. 403.
15. This summary Figure is obtained from U. Timm, presented at the 3rd Warsaw Symposium, Jodlowy Dwor, Poland, 1980, DESY 80/70. For detailed experimental references see this paper. G. Wolf (private communication) expects the $K^o_S \to \pi^+\pi^-$ correction to the TASSO data to yield an $\langle n \rangle$ correction of an amount similar to that found by the PLUTO group.
16. S. Pokorski and S. Wolfram, in preparation.
17. M. Basile et al., CERN-EP-180-113, 80-112, 80-111; Phys. Lett. 92B, 367 (1980).
18. See, for example, the talk by T. Coghen at this meeting; see also, R. Gottgens, et al., IC/HENP/79/27 (1980), submitted to Nucl. Phys.
19. A. Nandi, RL-80-046 (1980).
20. R. Brendelik et al., TASSO Collaboration, Phys. Lett. 89B, 418 (1980).
21. W. Thomé et al., Nucl. Phys. B129, 365 (1977).
22. The νp data is from Bell, et al., Phys. Rev. D19, 1 (1979) and from the BEBC Collaboration as summarized by N. Schmitz at the 9th Int. Symp. on Lepton and Photon Interactions, Batavia, Illinois, 1979.
23. I would like to thank S. Pokorski for a conversation on this point.
24. These curves are from N. Schmitz "Hadron Production by Neutrinos on Protons," presented at the XX Cracow School of Theoretical Physics, Zakopane, 1980, MPI-PAE/Exp. El. 88.
25. J. Whitmore, Phys. Rep. 27C, 187 (1976).
26. This section is based primarily on the work of Ref. 5. The other dual model approaches are very similar.
27. See J. F. Gunion, Phys. Rev. D12, 3469, (1975), and the more rigorous results of S. J. Brodsky and P. Lepage, SLAC-PUB-2478 (1980).

28. As discussed in Sec. I, this need not destroy quark counting; the number of radiated gluons is likely to be proportional to the number of valence quarks.
29. J. Berge et al., Phys. Rev. D18, 3905 (1978); M. Derrick et al., Phys. Rev. D17, 1 (1978) and references therein.
30. See the reviews at this Conference.
31. R. Blankenbecler and S. J. Brodsky, Phys. Rev. D10, 2973 (1974); J. F. Gunion, ibid., 242; G. R. Farrar, Nucl. Phys. B77, 429 (1974).
32. G. R. Farrar and D. R. Jackson, Phys. Rev. Lett. 35, 1416 (1975).
33. Point-like bremstrahlung diagrams were briefly considered in J. F. Gunion, Phys. Rev. D10, 242 (1974); later general counting rules for such diagrams were developed in R. Blankenbecler, S. J. Brodsky and J. F. Gunion, Phys. Rev. D12, 3469 (1975).
34. Full fragmentation predictions for point-like emission graphs were obtained by J. F. Gunion, Phys. Lett. 88B, 150 (1979), with special attention to the weak damping of exotic fragmentations.
35. See S. J. Brodsky and G. P. Lepage, Ref. 27; A. Mueller and S. Gupta, Phys. Rev. D20, 118 (1979) and A. Mueller's talk at this Conference; and G. Farrar and D. Jackson, Phys. Rev. Lett. 43, 246 (1979).
36. Van Chang, R. Hwa, OITS-138 (1980); R. Hwa's talk at this Conference; and Van Chang, R. Hwa, Phys. Rev. Lett. 44, 439 (1980).
37. This was the basic point of Ref. 34. For a highly detailed discussion of an $x \to 1$ limit in deep inelastic scattering see S. J. Brodsky and G. P. Lepage, Proceedings of Summer Institute on Particle Physics, SLAC, 1979.
38. J. Singh et al., CHLM Collaboration, Nucl. Phys. B140, 189 (1978).
39. R. Hwa's talk at this Conference and OITS-122 (1979) give the most recent versions of the Valon-recombination approach. E. Takasugi has done closely related work. See his talk at this Conference and E. Takasugi et al., Phys. Rev. D20, 211 (1979); Phys. Rev. D21, 1838 (1980).

40. D. Cutts et al., Brown-CERN-FNAL-INFN-MIT Collaboration, Phys. Rev. Lett. 42, 319 (1979); J. Saudraix et al., SACLAY-DPh DE 7803 (1978); Nucl. Phys. B149, 189 (1979); R. T. Edwards, et al., Phys. Rev. D18, 76 (1978); K. Böckmann, Symposium on Hadron Structure and Multiparticle Production, Kazimierz, 1977; W. Lockman et al., Phys. Rev. Lett. 41, 680 (1978); J. Singh et al., Nucl. Phys. B140, 189 (1978); Bodier et al., referenced in Bourquin, below; Hungerbühler et al., referenced in Bourquin, below; M. Bourquin et al., Nucl. Phys. B153, 13 (1979); J. R. Johnson et al., Phys. Rev. D17, 1292 (1978); Brussels-CERN-Genova-Mons-Nijmegen-Serpukhov-Tel Aviv Collaboration, submitted to 1979 EPS meeting ($K^+p \to \pi^-$); Aachen-Berlin-CERN-Cracow-London-Vienna-Warsaw Collaboration, submitted to 1979 EPS meeting (K^-p interactions); B. Alper et al., Amsterdam-CERN-Cracow-Munich-Oxford-Rutherford Collaboration, submitted to 1979 EPS meeting (inclusive ϕ production in K^+, K^-, π^+, π^-, p beams); I. V. Ajinenko et al., French-Soviet-CERN-Soviet Collaboration ($K^+p \to \pi^\pm$) IFVE-79-39, submitted to Nucl. Phys. and to 1979 EPS meeting; E. A. DeWolf et al., Belgium-Serpukhov Collaboration, submitted to 1979 EPS meeting (K^+p interactions). The Fig. 27 type of plot was first presented by R. Diebold, Proceedings of the 19th Int. Conference on High Energy Physics, 1978, edited by S. Homma et al., (Tokyo, Japan; Physical Society of Japan)p. 666. For recent summaries see also the reviews and presentations at this conference and by W. Kittel at the X Int. Symp. on Multiparticle Dynamics, Goa, 1979.

41. D. Denegri et al., France-Soviet Union-CERN Collaboration, "Inclusive Hadronic Fragmentation in $K^\pm p$ Interactions at 32 GeV/c and Quark Counting Rules," Brügge, 1980.